HIPPOCAMPUS 6:149–172 (1996)

Theta Phase Precession in Hippocampal Neuronal Populations and the Compression of Temporal Sequences

William E. Skaggs, Bruce L. McNaughton, Matthew A. Wilson, and Carol A. Barnes

ARL Division of Neural Systems, Memory and Aging, University of Arizona, Tucson, Arizona

ABSTRACT: O'Keefe and Recce [1993] Hippocampus 3:317–330 described an interaction between the hippocampal theta rhythm and the spatial firing of pyramidal cells in the CA1 region of the rat hippocampus: they found that a cell's spike activity advances to earlier phases of the theta cycle as the rat passes through the cell's place field. The present study makes use of large-scale parallel recordings to clarify and extend this finding in several ways: 1) Most CA1 pyramidal cells show maximal activity at the same phase of the theta cycle. Although individual units exhibit deeper modulation, the depth of modulation of CA1 population activity is about 50%. The peak firing of inhibitory interneurons in CA1 occurs about 60° in advance of the peak firing of pyramidal cells, but different interneurons vary widely in their peak phases. 2) The first spikes, as the rat enters a pyramidal cell's place field, come 90°–120° after the phase of maximal pyramidal cell population activity, near the phase where inhibition is least. 3) The phase advance is typically an accelerating, rather than linear, function of position within the place field. 4) These phenomena occur both on linear tracks and in two-dimensional environments where locomotion is not constrained to specific paths. 5) In two-dimensional environments, place-related firing is more spatially specific during the early part of the theta cycle than during the late part. This is also true, to a lesser extent, on a linear track. Thus, spatial selectivity waxes and wanes over the theta cycle. 6) Granule cells of the fascia dentata are also modulated by theta. The depth of modulation for the granule cell population approaches 100%, and the peak activity of the granule cell population comes about 90° earlier in the theta cycle than the peak firing of CA1 pyramidal cells. 7) Granule cells, like pyramidal cells, show robust phase precession. 8) Cross-correlation analysis shows that portions of the temporal sequence of CA1 pyramidal cell place fields are replicated repeatedly within individual theta cycles, in highly compressed form. The compression ratio can be as much as 10:1.

These findings indicate that phase precession is a very robust effect, distributed across the entire hippocampal population, and that it is likely to be inherited from the fascia dentata or an earlier stage in the hippocampal circuit, rather than generated intrinsically within CA1. It is hypothesized that the compression of temporal sequences of place fields within individual theta cycles permits the use of long-term potentiation for learning of sequential structure, thereby giving a temporal dimension to hippocampal memory traces. © 1996 Wiley-Liss, Inc.

KEY WORDS: CA1, fascia dentata, place cells, long-term potentiation, phase coding

Accepted for publication February 14, 1996.

Address correspondence and reprint requests to Dr. B. L. McNaughton, 344 Life Sciences North, University of Arizona, Tucson, AZ 85724. Dr. Wilson is currently at the Massachusetts Institute of Technology, Boston, Massachusetts.

The hippocampal theta rhythm, with a frequency range of 4–12 Hz, is one of the largest, most regular EEG rhythms in the rat brain, and has engendered decades of research (Jung and Kornmüller, 1938; Green and Arduini, 1954). Its generating mechanisms are complex and only partially understood, and its functional significance is unknown, though there have been many interesting speculations. In rats, the presence of theta rhythm with a characteristic frequency of 7–9 Hz is strongly correlated with what Vanderwolf et al. (1975) called type I movements, which include locomotion, orienting, rearing, or exploratory sniffing; a strong theta rhythm is also invariably present during REM sleep (Winson, 1972). During light dissociative anesthesia, and occasionally during still alert states, theta oscillations with a lower frequency range and distinctive pharmacological properties can be recorded (Kramis et al., 1975; Sainsbury et al., 1987). All types of theta are eliminated from the hippocampal formation if the medial septal area is lesioned or inactivated, but the sources and sinks of the extracellular electric currents are generated mainly in the CA1 layer, fascia dentata, and entorhinal cortex (for recent reviews see Vanderwolf and Leung, 1983; Buzsáki et al., 1983; Bland, 1986; Vanderwolf, 1988; Stewart and Fox, 1990; Bland and Colom, 1993).

O'Keefe and Recce (1993) discovered an interesting relationship between the theta rhythm and the spatially specific firing of hippocampal pyramidal cells. In many experimental situations involving freely moving rats, pyramidal cells of the CA1 and CA3 regions, and granule cells of the fascia dentata, have "place fields": each cell fires robustly when the rat is in a specific small portion of the environment, and is virtually silent when the rat is elsewhere (O'Keefe and Dostrovsky, 1971; O'Keefe, 1976; O'Keefe and Conway, 1978; Olton et al., 1978; McNaughton et al., 1983a; Jung and McNaughton, 1993). Place fields vary in size and shape, and if a sufficiently large population of cells is recorded, their place fields extend into every part of any given environment (O'Keefe and Nadel, 1978; Muller et al., 1987; Eichenbaum et al., 1989; Leonard, 1990; Wilson

and McNaughton, 1993). O'Keefe and Recce found that the phase of the theta cycle at which a pyramidal cell fires advances gradually as the rat passes through the cell's place field. This phenomenon is extremely interesting, because, by indicating that the phase at which a cell fires carries information, it holds some promise of revealing a computational function for the theta rhythm. In fact, Burgess et al. (1994) have developed a computational model of the role of the hippocampus in navigation, which depends critically on the phase shift to encode the geometric structure of the environment.

The experiments performed by O'Keefe and Recce left a number of important questions open, among them:

1. How robust is the phase precession effect in different experimental situations? Does the effect only appear on a linear apparatus where animals move along stereotyped trajectories, and where, in contrast to fully two-dimensional environments, firing depends strongly on head orientation?
2. Is the phase advance coherent across the CA1 population? In other words, do all cells begin to fire at the same phase of the theta cycle as the rat enters their place fields, or is the onset of firing variable with respect to theta phase? This question is important with regard to the effects of precession on the temporal structure of population activity, and was not addressed by O'Keefe and Recce (1993). It should be noted that Burgess et al. (1994) nevertheless assumed, without explicitly saying so, that the phase advance is coherent.
3. If the phase advance is in fact coherent across the CA1 population (as will be demonstrated in this paper), how does the "zero" point (i.e., the phase at which the first spikes occur) relate to the peaks and valleys of EEG waves recorded at various locations within the hippocampus, and to the global theta-modulation of hippocampal unit activity (Fujita and Sato, 1964; Artemenko, 1973; Buzsáki et al., 1983; Fox et al., 1986; Bland and Colom, 1993)?
4. Does phase precession occur only in CA1, or in other parts of the hippocampal formation as well? If it occurs at stages prior to CA1, then it may be inherited by CA1, rather than generated there.
5. What is the physiological mechanism of phase precession? O'Keefe and Recce proposed a model, involving two interacting oscillators with slightly different frequencies, but the evidence to support this was minimal.
6. What is the functional significance of phase precession, if any?

The studies reported in this paper were designed to give insight into these questions, with the aid of parallel recording techniques which permitted dozens of cells—including CA1 pyramidal cells, dentate gyrus granule cells, and interneurons in both areas—to be recorded simultaneously. Some of the results have previously been reported in abstract form (Skaggs et al., 1993b).

MATERIALS AND METHODS

Surgery and Recording

The data for this study were recorded from eight male Fisher 344 rats, each approximately 9 months old. The rats were maintained on a 12:12 hour light-dark cycle, with most recordings made during the dark portion of the cycle. During recording, three of the rats foraged for scattered food pellets in an open arena; the other five ran for food reward on a triangular track. To motivate behavior, the animals were food-deprived to approximately 85% of their ad libitum weights before training.

The first three rats, prior to electrode implantation, were extensively trained to forage for randomly scattered food pellets. For two of the rats, the apparatus was a 60 cm square box with high, opaque walls. For the third rat, the apparatus was an open rectangular platform, 80 cm long and 30 cm wide, with an opaque barrier at one end. After surgery, the rats were retrained in the task; by the time the data used here were recorded, each rat was prepared to spend well over half an hour foraging, with few pauses. For the second group, the rats were also extensively trained prior to surgery. The maze was an elevated wooden triangle, with each side 75 cm long and 8 cm wide. The rats were given food reward at the center of each side, and for a given session (training or recording), they were required to move only in a single direction (clockwise or counterclockwise).

For electrode implantation, the rats were deeply anesthetized with Nembutal and placed in a stereotaxic apparatus. All surgical procedures were performed in accordance with NIH guidelines. The skin over the skull was incised and retracted. Several holes were drilled for jeweler's screws; then a circular hole was drilled over the dorsal hippocampus on the right side of the brain, at coordinates approximately 3.5 mm posterior to bregma, 2.0 mm lateral to the midline. The dura was slit and retracted, and the electrode array was positioned with the electrode tips a short distance into the brain, and cemented in place with dental acrylic.

The electrode array consisted of 13 or 14 independently movable "tetrodes," 12 of which were used for unit recording and one as a reference for differential recording. In the 14-tetrode arrays (used in five rats), the extra tetrode was used specifically for recording EEG. Each tetrode consisted of four polyimide-coated 13-μm nichrome wires, twisted together and cut so that the tips were parallel. The tips were then gold-plated, usually yielding resistances in the range 300–600 kΩ. Each tetrode was inserted into two nested plastic support cannulae, 78 and 110 μm in diameter, which were themselves inserted into a 30-gauge stainless steel cannula. The stainless steel cannula was bent at a 30° angle near the end; this allowed the tips of all the tetrodes to be placed within an area less than 2 mm across, while the other ends fanned out into a cone, giving enough separation so that the tetrodes could be individually manipulated without interference. Each 30-gauge cannula was attached, using a "nut" made of dental acrylic, to a metal screw, which could be turned to raise or lower the corresponding tetrode. One turn of the screw equaled approximately 320 μm in depth. Each tetrode wire was attached with silver paint to a contact point on a multiple-pin connector plug.

For recording, the connector plug was attached to a custom-build headstage (Fig. 1) containing two commercially available microchips (Multichannel Concepts, Inc., Gaithersburg, MD), each with 25 unity-gain FET amplifiers, for impedance reduction. The headstage was in turn attached to a multistrand, fine-wire cable, which carried the signals to a set of seven custom-de-

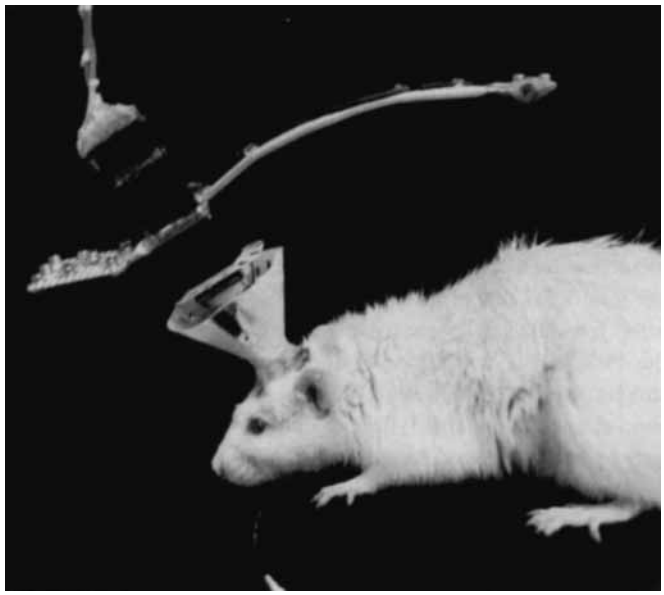

FIGURE 1. Photo of rat with implanted electrode array (within protective cone) and headstage attached. Extending from the headstage are two arrays of light-emitting diodes, a large array in front, and a smaller array about 15 cm behind. The headstage was plugged into a suspended multistrand fine-wire cable during recording.

signed, eight-channel, software-controlled amplifiers, and thence to a group of seven 80486-based microcomputers. The signal from each tetrode wire was amplified by a factor of 10,000 and filtered with a bandpass of 600–6000 Hz, before being sent to A/D cards (Data Translation, Inc., Marlboro, MA) on the microcomputers. The data were recorded using *Discovery* data acquisition software (BrainWave Inc., Broomfield, CO), specially modified for parallel recording. Each tetrode channel was monitored at a rate of 32 KHz, and whenever the amplitude of the signal exceeded a predetermined threshold (which could be set independently for each tetrode channel), a 1-ms sample of data was acquired from all four channels of the tetrode. These spike samples were timestamped and stored on hard disk. The timestamp clocks had a resolution of 100 μsec, and were synchronized by a clock signal emitted from one of the seven computers, which served as master controller. Signals from eight of the tetrode channels (which could be chosen arbitrarily) were additionally sent to another eight-channel amplifier, where they were amplified by a factor of 2000 and filtered with a bandpass of 1–100 Hz or 1 Hz–3 KHz, then sampled continuously at a rate of 250 Hz or 1000 Hz, and stored on hard disk. These additional channels were used to record EEG.

Also attached to the headstage were two small arrays of infrared LEDs, used for position tracking. The front diode array was located in front of the rat's nose, approximately 5 cm up. A second, smaller diode array extended about 15 cm back from the headstage on a small "boom." The two sets of diodes taken together allowed both the location and head direction of the rat to be tracked. Position data were acquired by a video camera mounted in the ceiling of the recording area, and sent to a tracking device (Dragon Tracker model SA-2, Boulder, CO), which extracted and stored the coordinates of all pixels whose intensity exceeded an adjustable threshold, at a resolution of 256 × 256 pixels. This information was sent, at a rate of 20 frames per second, to one of the microcomputers, in which the *Discovery* software calculated the coordinates of the largest and second-largest "blobs" of active pixels, which were taken to represent the front and rear diode arrays, respectively. These data were recorded on disk, and later reprocessed off-line, with custom-written software on a Sun workstation, to correct or delete occasional points in which the two diode arrays were reversed, or otherwise misidentified. The videocamera placement for these experiments gave a resolution of 1.8 pixels/cm for the rectangular boxes, and 2.3 pixels/cm for the triangle maze; however, the average uncertainty in position tracking, due to the size of the diode arrays, the distance of the diodes above the rat's head, and variations in posture, was estimated at about 5 cm in both environments.

At the conclusion of a recording session, the data were transferred from the seven microcomputers to a Sun workstation for further processing steps, including unit identification and isolation. The principle of tetrode recording was proposed by McNaughton et al. (1983b) as an extension of the stereotrode recording method, and is described in detail by O'Keefe and Recce (1993). Briefly, a tetrode is an electrode consisting of four microwires twisted together and cut in parallel, resulting in tips so closely spaced that most cells picked up by any of the wires will simultaneously be picked up by one or more of the other wires. Different cells are distinguished on the basis of the relative amplitudes of their spikes on the four wires, with the largest signals appearing on the wire whose tip lies nearest to the soma of a cell. Using this principle, as many as 20 cells (but more typically five to ten) can be isolated from a tetrode placed in the CA1 layer of the rat hippocampus, where the tight packing of cells makes it difficult to separate units using conventional single electrode recording methods.

Unit identification and isolation were performed using a technique called "cluster-cutting" (McNaughton et al., 1989), by means of custom-written software employing an X-window based graphical interface. The method of isolation was to calculate for each spike a small set of N waveform parameters (the peak heights on the four tetrode channels being the most important), thus deriving from each spike a point in N-dimensional parameter space. The cluster-cutting software allows the set of parameter points to be projected onto two-dimensional subspaces, and displayed as scatterplots on the computer screen. When this is done, points deriving from a single cell tend to form recognizable clusters. The user isolates these clusters by defining polygonal borders around them, with a mouse. Typically a cell is identified by drawing a border around a cluster of points in the two-dimensional projection in which it is most clearly distinguishable from other clusters, and then isolated more cleanly by adding boundaries in other projections. At the end of this process, a unit is defined by the conjunction of boundaries drawn in several planes of projection.

After the rats had recovered from surgery, the 12 tetrodes were gradually lowered, over the course of several days, into the CA1 cell body layer of the dorsal hippocampus. This was recognized

by several criteria, including the presence of 100–300 Hz "ripples" in EEG recorded from the tetrodes (O'Keefe, 1976; O'Keefe and Nadel, 1978; Buzsáki et al., 1992; Ylinen et al., 1995), "sharp waves" in the EEG which reverse polarity about 50 μm below the CA1 layer (Buzsáki et al., 1986; Suzuki and Smith, 1987), and most importantly, the sudden appearance, at a depth about 2 mm below the dura, of large numbers of simultaneously recorded cells firing complex spikes. In a number of cases, individual tetrodes were lowered past the CA1 layer, to the dorsal blade of the fascia dentata. This layer can be recognized by a combination of unit activity from multiple low-rate cells firing occasional complex spikes, strong gamma-band (30–70 Hz) activity in the locally recorded EEG, and low-amplitude theta waves. These criteria are not as uniformly reliable as those for CA1, but if they are satisfied, the probability that the electrode is in the granular layer of the fascia dentata is reasonably high.

Pyramidal cells were distinguished from theta cells in the CA1 region by a number of criteria (Ranck, 1973; Fox and Ranck, 1981; Buzsáki et al., 1983; McNaughton et al., 1983a). To be classified as a pyramidal cell, a unit was required to 1) be recorded simultaneously with other pyramidal cells; 2) fire at least a small number of complex spike bursts during the recording session; 3) have a spike width (peak to valley) of at least 300 μsec; and 4) have an overall mean rate below 5 Hz during the recording session. To be classified as a theta cell, a unit was required to 1) fire no complex spike bursts; 2) have a spike width less than 300 μsec; and 3) fire with a mean rate above 5 Hz during the recording session.

Granule cells of the fascia dentata were recognized according to a set of criteria derived largely from the findings of Jung and McNaughton (1993). These were that 1) the cell must have a low mean rate and fire complex spikes at least occasionally; 2) the recording electrode must have passed through the CA1 layer, and then been lowered several hundred microns farther; 3) EEG sampled from the recording electrode must show strong activity in the gamma band (30–80 Hz), together with a weak or absent theta signal; 4) at least one other low-rate cell firing some fraction of complex spikes must be recorded together with the cell in question, from the same tetrode. Theta cells in the fascia dentata were classified according to the same criteria used for theta cells in CA1.

Quantification of Theta Rhythm

Ideally, EEG would have been recorded in all cases from an electrode placed near the hippocampal fissure, or else 200–300 μm above the CA1 layer, because theta recorded at these locations is large in amplitude and relatively insensitive to small variations in electrode position. The extra recording channel necessary to accomplish this was not, however, available in the first three data sets used in this study; nevertheless with appropriate measures (described in this section), it proved possible to obtain meaningful results with the lower quality theta signal that can be recorded in the vicinity of the CA1 pyramidal layer.

In the first three data sets used for these studies (those involving foraging in a rectangular arena), EEG was recorded continuously from eight tetrodes, selected from among the 12 used for recording unit activity. For one of these sessions, the EEG signals were filtered with a bandpass of 1–100 Hz and sampled at 250 Hz; for the other two sessions the signals were filtered at 1–3,000 Hz and sampled at 1,000 Hz. (No intermediate filter settings were available with our apparatus.) The latter settings will have caused power in the 500–3000 Hz range to be aliased into the sampled data, but this is unlikely to have caused significant distortion in the theta band. In general, only a small fraction of the total EEG power falls within the 500–3000 Hz band. In the other five data sets (those involving running on a triangle-maze), the 14th tetrode was exploited to record EEG approximately 300 μm below the CA1 cell body layer, near the fissure dividing CA1 from the fascia dentata. These signals were filtered with a bandpass of 1–100 Hz and sampled at 250 Hz.

During locomotor behavior and REM sleep, a theta rhythm at a frequency of approximately 8 Hz could usually be observed on all channels. The amplitude of the signal varied considerably between sites, and so did the phase, but the phase difference between any given pair of channels appeared consistent over time. The channel having the strongest and least noisy theta component was determined, and digitally filtered, using an FFT, into the 6–10 Hz band. (For the triangle maze data, the EEG electrode near the CA1-dentate fissure was always used.) Figure 2 shows examples of raw and filtered EEG. There is no generally accepted criterion for determining when a theta rhythm exists; for our purposes, theta was deemed to exist at any point at which the preceding and following peaks of the filtered signal were separated by between 100 and 200 ms, with each peak exceeding a specified threshold. The threshold was set such that, for the most part, theta was only deemed to be present when a theta-frequency oscillation in the EEG was obvious to the eye. The pattern of results we observed was not substantially altered even by rather large changes in the threshold. The frequency range for theta during maze-running is commonly stated as 7–12 Hz, or even 7–14 Hz, so it might be thought that a significant fraction of theta would be lost or distorted. In our data, however, only a small fraction of theta oscillations fell outside the range 7–9 Hz.

Each spike, if theta existed when it occurred, was assigned a nominal phase, according to the fraction of the time between the preceding and following theta peaks at which it occurred. Precisely, the phase assigned to an event at time t was $360 \cdot (t - t_0)/(t_1 - t_0)$, where t_0 and t_1 are the times of the preceding and following peaks of the filtered reference EEG signal. Note that the phase was always a number between 0 and 360.

To make the phase data comparable across animals, it was necessary to adjust these nominal phase values. The necessity arises from the fact that theta waves recorded at different points in the hippocampal formation, while always very strongly phase-locked, do not always peak simultaneously. In our data, the peaks were sometimes shifted by as much as 45° even for electrodes all located near the CA1 cell body layer. This is probably a consequence of the existence of multiple generators that summate in different ways at different locations (Buzsáki et al., 1983; Leung, 1984). To compare phases across animals, we made use of the fact (established in the Results section of this paper; see also Fox

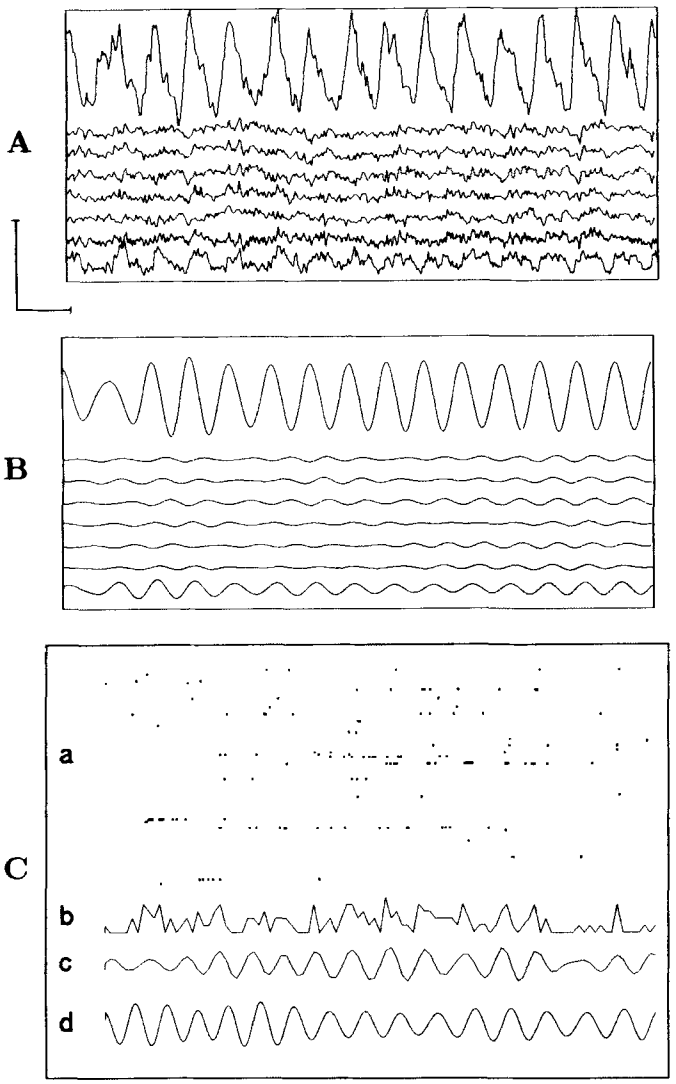

FIGURE 2. Examples of raw and filtered EEG, together with CA1 pyramidal cell population activity. A: A typical example of EEG recorded simultaneously from eight electrodes, one located several hundred μm below the CA1 layer (top trace), the other seven located in or near the CA1 layer, in a rat running on the triangle maze. Filter bandpass: 1–100 Hz. Scale bar: 1 mV, 200 ms. B: The EEG signal from A, digitally filtered with a bandpass of 6–10 Hz. The peaks of the reference channel (top trace) were used to compute phases of the theta cycle for the analyses performed here. C: Example of CA1 pyramidal cell activity in relation to the theta rhythm. a, Raster plot of two seconds of spike activity from 117 simultaneously recorded CA1 pyramidal cells, in a rat foraging for scattered food pellets. Many of the cells are silent. (Silent cells in this and subsequent figures were isolated on the basis of activity during sleep before and after the maze-running session.) b, Summed activity of the pyramidal cells, using a bin size of 20 ms. c, The trace from b, filtered with a 6–10 Hz bandpass and amplified by a factor of 2. d, The reference EEG signal, filtered with a 6–10 Hz bandpass. Note the strong coherence between the signals in c and d.

et al., 1986, and Buzsáki et al., 1983) that hippocampal pyramidal cell population activity is modulated in a consistent way by the theta rhythm, with the peak occurring simultaneously throughout the dorsal hippocampus (CA1 and probably CA3 as well). Global phase zero was defined to be the point in the theta cycle corresponding to maximal pyramidal cell activity. Thus, we measured the theta rhythm using EEG, and used population pyramidal cell activity, integrated across an entire data set, to decide which point on the EEG wave to call phase zero.

Spatial Firing Measures

Three measures were used to quantify the sharpness of spatial tuning of a spike train, *spatial information per spike* (Skaggs et al., 1993a), *sparsity*, and *selectivity*.

The spatial information per spike is derived by considering the cell as a communication channel whose input is the rat's location and whose output is the cell's spike train; the derivation assumes that all of the information is conveyed by the cell's instantaneous firing rate. Intuitively, if a cell fires across half of an environment, then the occurrence of a spike conveys one binary bit of information about the rat's location. If the cell fires in one quarter of the environment, a spike conveys two bits of information, and so on. The formula is:

$$Information = \sum_{i=1}^{N} p_i \frac{\lambda_i}{\lambda} \log_2 \frac{\lambda_i}{\lambda},$$

where the environment is divided into nonoverlapping spatial bins $i = 1, \ldots, N$, p_i is the occupancy probability of bin i, λ_i is the mean firing rate for bin i, and λ is the overall mean firing rate of the cell.

The sparsity measure is an adaptation to space of a formula invented by Treves and Rolls (1991); the adaptation measures the fraction of the environment in which a cell is active. Intuitively, a sparsity of, say, 0.1 means that the place field of the cell occupies 1/10 of the area the rat traverses. The formula is:

$$Sparsity = \frac{\langle \lambda \rangle}{\langle \lambda^2 \rangle} = \frac{(\sum p_i \lambda_i)^2}{\sum p_i \lambda_i^2},$$

where the angle brackets ($\langle \cdot \rangle$) denote the expected value averaged over locations. The sparsity of a firing rate map is closely related to the spatial coefficient of variation of the firing rates; if C is the coefficient of variation, then the relation is,

$$Sparsity = \frac{1}{1 + C^2}.$$

The selectivity measure is equal to the spatial maximum firing rate divided by the mean firing rate of the cell. The more tightly concentrated the cell's activity, the higher the selectivity. A cell with no spatial tuning at all will have a selectivity of 1; there is in principle no upper limit. A similar measure was used by Barnes et al. (1983), except that the "out-of-field" firing rate was used instead of the mean rate. The present definition is preferable because it does not depend on identifying a "place field," and because it is much less sensitive to noise.

The information and sparsity measures have much in common—usually the information per spike is approximately equal to minus the logarithm (base 2) of the sparsity. Both of them tend to be more reliable than the selectivity measures, because the spa-

tial maximum firing rate is difficult to measures with great accuracy.

The spatial firing rates λ_i were calculated using an "adaptive binning" technique designed to optimize the tradeoff between sampling error and spatial resolution. The data were first binned into a 64 × 64 grid of spatial locations, and then the firing rate at each point in this grid was calculated by expanding a circle around the point until the following criterion was met:

$$N_{spikes} > \frac{\alpha}{N^2_{occ} r^2},$$

where N_{occ} is the number of occupancy samples (sampled continuously at 20 Hz) falling within the circle, N_{spikes} is the number of spikes emitted within the circle, r is the radius of the circle in bins, and α is a scaling parameter, set at 1.0×10^6 for these data sets; the firing rate assigned to the point is then $20 \cdot N_{spikes}/N_{occ}$. Since the proportional level of error of this technique is influenced by the overall firing rate of a cell (higher rates mean proportionately less error), when comparing specificity between different portions of the theta cycle, we used only a subset of spikes from the portion with higher activity, so that the sizes of the two samples were equalized. Empirical testing has indicated that the spatial information and sparsity measures are usually reliable to within 20% if the sample includes at least 50 spikes and every portion of the environment has been visited several times; but the validity of the current results do not depend strongly on this.

RESULTS

The data for these studies were recorded from three rats running for food reward in a rectangular arena, and another five rats on a triangular track. The number of CA1 pyramidal cells from each rectangular arena data set used for spatial specificity comparisons were 8, 13, and 26, respectively. Many more pyramidal cells were recorded from each data set, but were not considered sufficiently active for accurate spatial specificity measures to be calculated during the less active portion of the theta cycle. Three triangle maze data sets were also used for this purpose, with 47, 53, and 17 active cells, respectively. It was much easier to obtain adequate sampling for these cells, because the rats traversed each point on the maze many times, always facing in approximately the same direction. All dentate gyrus granule cells were recorded on the triangle maze; there were 37 of these with activity on the maze, recorded from three rats, in two of which CA1 pyramidal cells were recorded at the same time.

Theta Modulation of CA1 Pyramidal Cell Population Activity

In these tasks, a strong, regular theta rhythm was invariable present when the rats were engaged in locomotion. As illustrated in Figure 2C, the population activity of CA1 pyramidal cells was continuously modulated by the theta rhythm. The modulation is often difficult to see in a raster plot of pyramidal cell activity, and even in a plot of the summed activity of more than 100 cells, but it can easily be seen when the summed activity trace is filtered such that only the theta-frequency components remain.

A clearer picture of theta modulation of pyramidal cell population activity can be obtained by summing over a large number of theta cycles. Figure 3 plots the overall firing rates of two sets of simultaneously recorded CA1 pyramidal cells, as a function of phase of the theta cycle. The first set was recorded during quasi-random foraging in the rectangular box, the second set during running on the triangular track. In the rectangular box data, virtually all of the active cells showed peak activity at approximately the same point in the theta cycle. There were a few small, but reliable discrepancies, and two apparently otherwise normal pyramidal cells that showed peak activity 180° opposed to the population. In the triangle data there was considerably more variability; nevertheless the majority of cells showed peak activity clustered near one particular phase of the theta cycle. These differences in consistency of tuning were seen as well in data recorded from other rats in the rectangular box and triangle environments, and may be due to differences in behavior. On the triangle maze, the majority of a rat's time was spent consuming the food reward at the goal locations, whereas in the rectangular box, the majority of time was spent searching for food. In any case, regardless of the apparatus, the phase of peak population activity was well-defined, and consistent across different tetrodes which were spread over an area about 2 mm in diameter; the depth of modulation (peak − valley/peak) was generally around 50%.

Most data sets included a few theta cells, in addition to pyramidal cells. Because of the smaller number of theta cells in a given sample, it was not possible to reconstruct the phase relationship of the population of theta cells in the same manner as was done for pyramidal cells (i.e., using only cells recorded simultaneously). However, if the peak of pyramidal cell population activity is used as a reference for comparisons across animals, it appears that the relations of theta cells to the theta rhythm are less consistent than for pyramidal cells (Fig. 4). For a sample of 37 theta cells lying in or near the CA1 pyramidal layer, the distribution of peak phases was skewed such that activity overall was low early in the theta cycle, and increased progressively over the second half of the cycle. The activity of each theta cell varied in an approximately sinusoidal manner across the theta cycle, but the depth of modulation, and some of the behavioral correlates, for theta cells were highly variable. If this group of cells forms a representative sample, then the peak activity in the theta cell population probably occurs approximately 60° phase advanced to the peak of the pyramidal cell population; however, although many individual cells were strongly modulated, the estimated depth of modulation for cumulative inhibitory cell population activity is less than 20%, at least for those classes of interneurons whose somata are located in or near *stratum pyramidale.*

The O'Keefe-Recce Phase Precession Effect

O'Keefe and Recce (1993), examining EEG and single unit activity in rats running for food reward on a linear track, found a systematic relation between phase of the theta cycle and the part

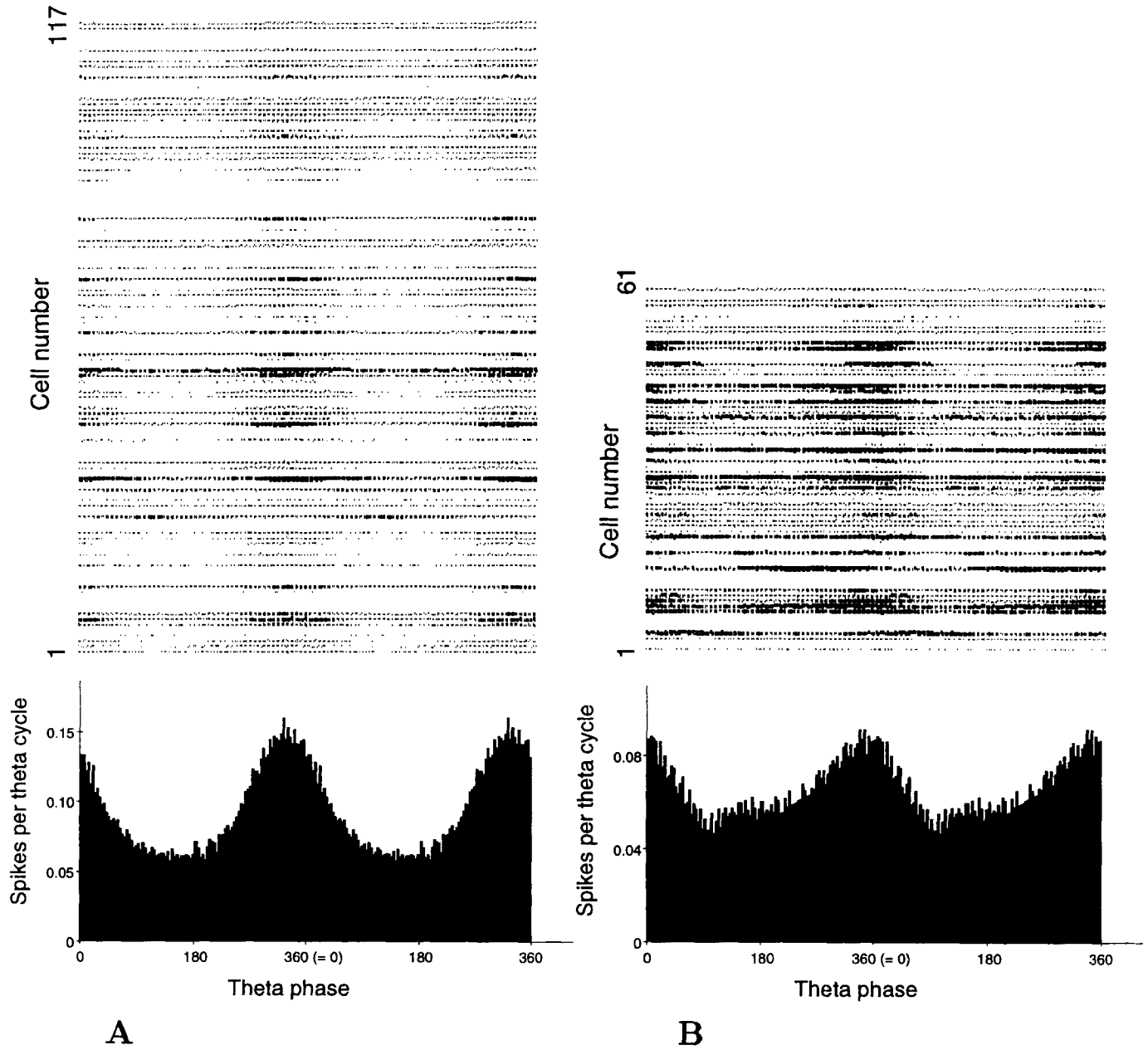

FIGURE 3. Theta modulation of CA1 pyramidal cell firing rates. A: Data from 117 simultaneously recorded cells, averaged over 10 min of foraging for scattered food pellets on an open platform. B: Data from 61 simultaneously recorded cells, averaged over 55 min of running for food reward on a narrow triangular track. Top: Each horizontal trace represents a single cell, with the size of the black rectangle proportional to the firing rate of the cell. The X axis represents phase, measured according to the peaks of the filtered reference EEG signal. (Note that in all later figures, but not this one, phase is measured with respect to the point of maximum pyramidal cell population activity.) The full theta cycle is repeated twice, so that edge effects will not obscure the pattern. Bottom: Pyramidal cell population firing rate as a function of phase of the theta cycle. Each histogram represents the same data as shown on top, summed across cells.

of a cell's place field in which the rat is located at the moment the cell fires. Specifically, they reported that spikes advance to earlier phases of the theta cycle as the rat passes through the place field. On linear mazes, where rats move along constrained paths, the basic observation is quite robust and easy to replicate, as illustrated in Figure 5. In our data, whenever place fields were located in portions of the environment where the rat moved consistently and reliably forward, e.g., the center of a linear runway, the phase shift effect was invariably present.

Figures 6A–D illustrate the phase precession effect in a different way. For each of four CA1 pyramidal cells active on the triangle maze, a point was chosen near the center of the cell's place field, and a histogram constructed to show the net activity of the cell in relation to the theta rhythm, aligned according to the mo-

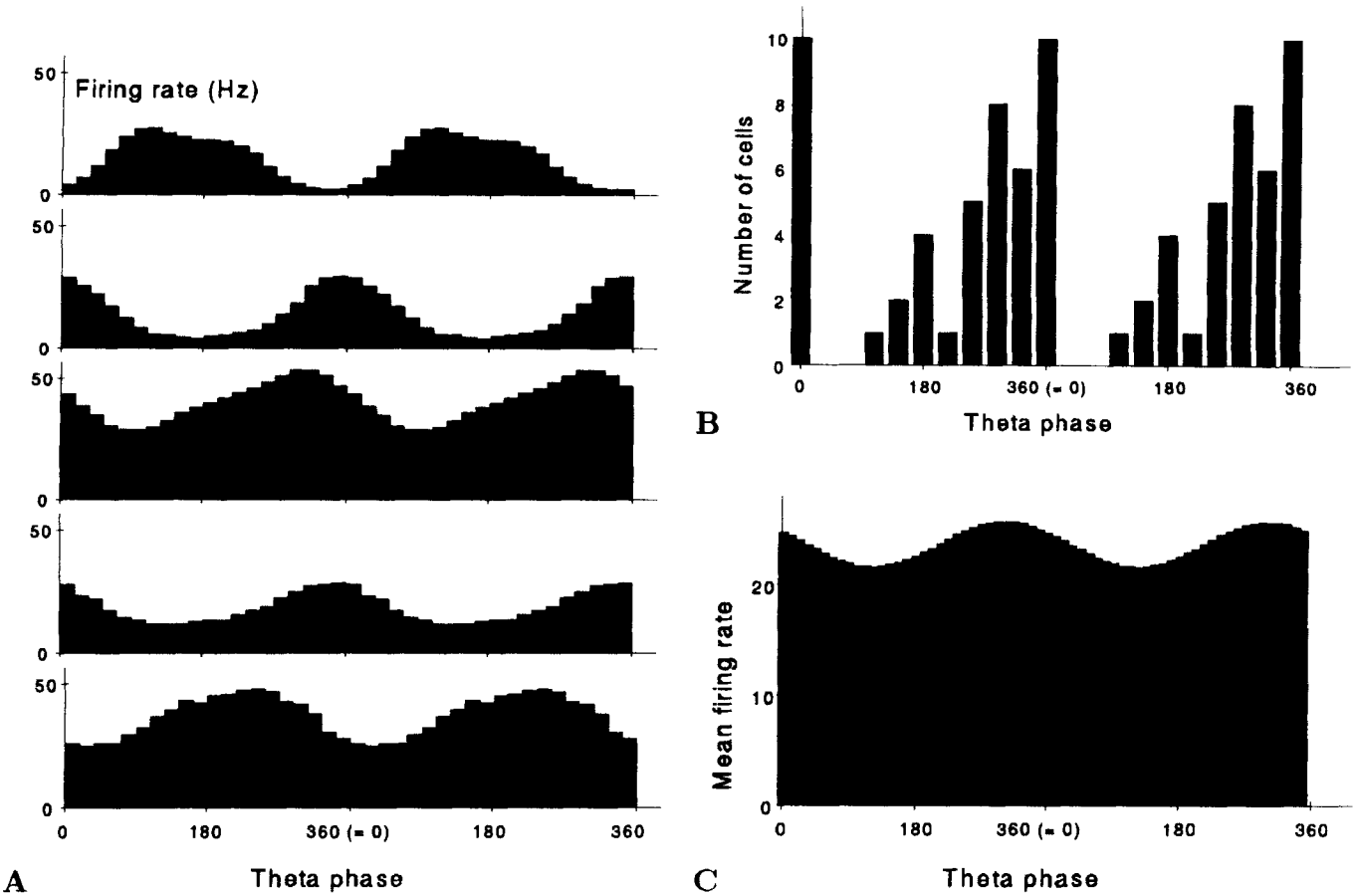

FIGURE 4. **Relations between the theta rhythm and firing rates of inhibitory interneurons. A: Examples of theta modulation of CA1 theta cell firing rates, for five theta cells recorded simultaneously in or near the CA1 cell body layer. B: Distribution of maximal-firing phases for a set of 37 theta cells recorded in or near the CA1 cell body layer, from several data sets. Each bar shows the number of cells whose maximal firing rate occurred at that phase of the theta cycle. The depth of modulation for these cells was highly variable. C: Estimated theta modulation of total CA1 theta cell activity, calculated by combining the phase data plotted in B with the measured depth of modulation of each cell. The estimated phase of maximal theta cell population activity is 58° in advance of the phase of maximal pyramidal cell activity, and the estimated depth of modulation is 17%.**

ment at which the rat passed the chosen point. In accordance with Figure 5, the illustrations show bursts of spike activity advancing to earlier phases as the rat passes through the place field. They also show that the true cycle-to-cycle depth of theta modulation of pyramidal cell activity is much greater than the overall average, and that the bursts of spikes first broaden and then narrow. The lesser modulation seen in the time-averaged data is at least partly due to the blurring effect of the phase precession. In addition, there is a tendency for some cells (e.g., Fig. 6B, C, and D) to show a certain amount of bimodal activity near the centers of their place fields. Note that the mean firing rates of these cells can exceed 100 Hz at the optimal combination of spatial location and theta phase.

Figures 5, 6, and 7 also illustrate an additional finding: every cell fires its first spikes, as the rat enters the place field, at approximately the same point in the theta cycle. This point invariably lies 90°–120° after phase zero (defined as the phase of peak population activity; see Materials and Methods), although there are small but reliable variations across cells (less than 30°). As Figure 4 indicates, this is actually near the phase where the estimated inhibitory cell activity is minimal, and, as Figure 3B indicates, it is in some cases near the phase of minimum pyramidal

FIGURE 5. **Phase precession of spike activity for three simultaneously recorded cells, on a triangle maze. A: Spatial distribution of theta peaks, in a rat running for food reward on the maze. Each point represents the location of the rat (front diode array) at the time of one peak of the recorded theta signal. The rat traveled for 55 min counterclockwise, completing 131 circuits of the maze. The three dense clusters of points represent reward locations, where the rat invariably stopped for a few seconds to eat. B, C: Examples of theta-related shifts in spatial firing. Each panel represents data from one CA1 pyramidal cell; both cells were recorded during the same session shown in A, and had place fields on the triangular maze. Gray dots show the rat's trajectory. Each colored circle shows the rat's location at the moment of a single spike; the small line coming out of the circle indicates the rat's head direction. The key (lower left) gives the relationship between colors and phases of the theta cycle—i.e., green and blue correspond to the phase with highest pyramidal cell population activity. D: Theta-related shift in spatial firing for a granule cell of the fascia dentata, recorded simultaneously with the two cells shown in B and C, whose place field closely matched that of the CA1 pyramidal cell used for panel C. The main difference between the pyramidal cell in C and the granule cell in D is that the granule cell shows very few blue spikes; that is, the first spikes emitted, as the rat enters the place field, fall about 90° earlier in the theta cycle than the first spikes emitted by the pyramidal cell. This lack of activity at the end of the theta cycle was characteristic of the granule cells recorded in this study.**

cell population activity. In the examples illustrated in Figure 5, the cells fire their last spikes, as the rat exits the place field, approximately 120° after phase zero, giving rise to a net phase shift approaching 360°, as reported by O'Keefe and Recce. This is not, however, an inevitable occurrence. As illustrated in Figure 7, cells always begin firing at approximately the same theta phase, but some, particularly those with very weak fields (e.g., cells 3, 6, 9, 10, 23, 25, 28, and 35), show only a small phase shift by the time

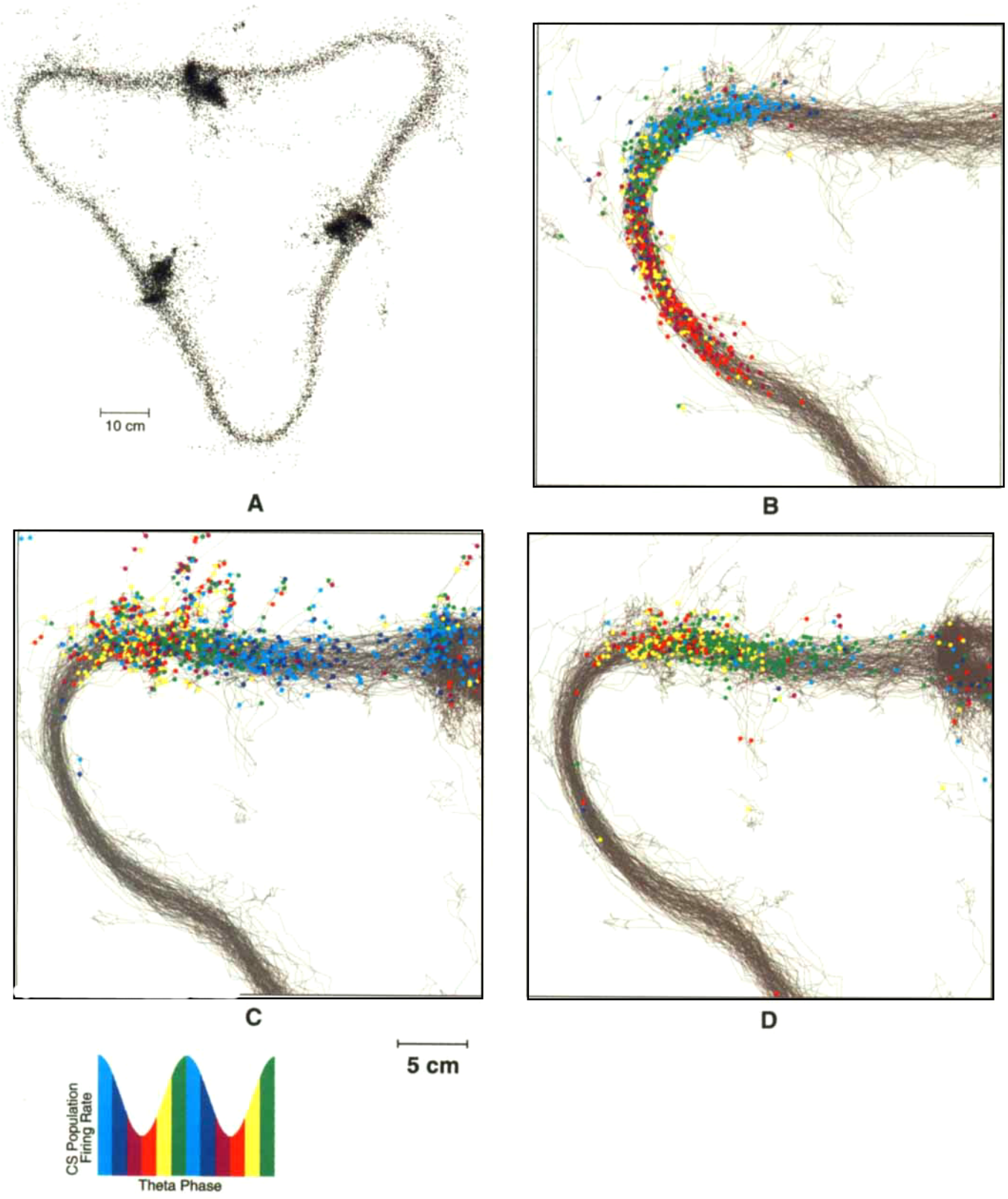

firing ceases. Also apparent in Figure 7 is the fact that when the place field impinges on a reward location, where the animal typically stops for a few seconds, firing appears to spread across the entire theta cycle. It is difficult to rule out, however, that this effect may partly result from error in estimating phase as a consequence of lower amplitude or absence of theta waves while the animal eats. It could also partly reflect a tendency of the animal to swing his head from side to side while at a reward location.

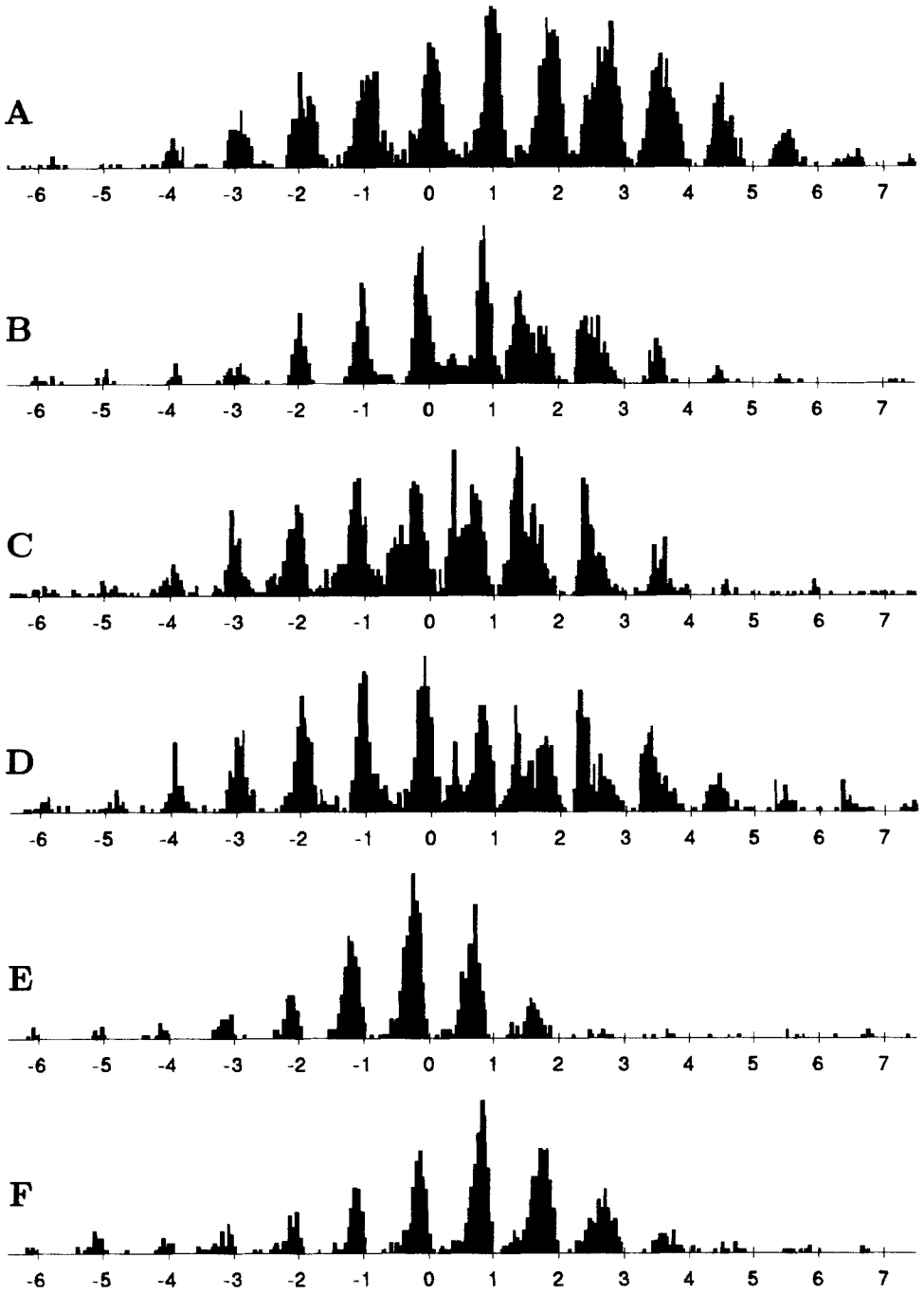

FIGURE 6. Phase precession of spike activity for four CA1 pyramidal cells (A, B, C, D) and two dentate gyrus granule cells (E, F), all recorded during the same session as those shown in Figure 5. Each histogram was constructed by choosing a point near the center of the cell's place field, and aligning each spike fired by the cell in terms of its theta phase and the number of cycles before or after the rat passed the chosen point. Bin size = 0.05 theta cycles. Tick marks indicate the phase corresponding to maximal pyramidal cell population activity. Note that in each example, the centers of the bursts precess steadily leftward with respect to the tick marks. For the CA1 cells, the first bursts are centered shortly after the tick marks, and the last are centered midway between the marks. For the granule cells, in contrast, the first bursts are centered shortly before the tick marks. The scale of the largest bar ranges from 80 to 110 total spikes in these histograms (approximately 90–120 Hz).

We do not find that in the majority of cases it is adequate to describe the phase shift as a simple linear advance. Figure 7 shows phase vs. location plots for a group of cells recorded simultaneously on the triangle. Clearly there is a great deal of variability here; but several points deserve to be noted. First, the phase advance sometimes accelerates as the rat moves through the place field; i.e., the plotted points form a downward curve rather than a straight line, as in cells 1, 14, 18, and 34. Second, the precession of the onset of firing within each cycle occurs more rapidly than the precession of the termination of firing; i.e., the cluster of points broadens vertically as one passes through the place field from left to right, e.g., cells 4, 17, 30, and 36. At about the middle of the field, the firing of many cells spans the entire theta cycle. Third, as previously noted, weakly active cells often do not show as much phase precession as strongly active ones, e.g., cells 3, 6, 9, 10, 23, 25, 28, and 35. Fourth, in many cases the points are concentrated in two or more distinct clusters, corresponding to different theta phases and different locations, rather than shifting smoothly and evenly, e.g., cells 5, 13, 14, 18, 24, and 29. Fifth, there are several cells for which a double phase advance pattern appears, e.g., cells 12, 29, 32, 33, 38, 39, and 40. It is possible that one or more of these represent two cells that could not be distinguished on the basis of their waveforms on any tetrode channel, with adjoining place fields, but it is extremely unlikely that this would happen seven times in a single data set. (These cells could be said to show a phase advance greater then 360°, but in every case it is a discontinuous phase advance.) A few of the patterns displayed here might reasonably be described in terms of a linear phase advance (e.g., cells 4, 19, 27, and 38), but the majority clearly show more complex dynamics.

It might be supposed that the phase precession could be accounted for, at least in part, by a systematic relation between theta phase and the rat's spatial location. This is not an unreasonable conjecture, because it has been reported that several types of movement are correlated with particular phases of the theta cycle (Macrides et al., 1982; Semba and Kornisaruk, 1978; Buño and Velluti, 1977); however, as illustrated in Figure 5A, if any such effects occur in our data, they are beyond the resolution of the position-tracking system employed in these studies. The spatial distribution of theta peaks does not show any recognizable tendency to form distinct clusters (except at the reward locations, where the rat spends most of its time). Figure 5A does not rule out a relation between theta phase and location, but it does demonstrate that any such relation cannot explain the phase precession of spatial firing.

Two-Dimensional Environments

The experiments described thus far, and those performed by O'Keefe and Recce (1993), used environments in which the rat was constrained to move along more or less specific trajectories: a linear track or a triangle maze. We have also examined the effects of theta phase on spatial firing in environments where the rat is permitted to move freely in a properly two-dimensional region of space.

As Figure 8A illustrates, the pattern of phase shifting is much less obvious in this case. When the spatial firing pattern is plotted in the same way as before, it is difficult to discern any systematic differences in the distribution of colors. Nevertheless, a phase precession effect can be demonstrated, by simplifying the color scheme. The remainder of the figures in this section use only two colors. Blue indicates the portion of the theta cycle beginning 60° before the peak of pyramidal cell population activity and ending 120° after the peak. This is the portion containing the earliest firing on a linear track. Red indicates the other half of the theta cycle, which contains the last spikes, as the rat leaves the place field, on a linear track. (These match the usage of blue and red in the earlier figures.)

As demonstrated in Figure 8B (illustrating a very strong, but not otherwise atypical, place field), there are clear differences in the spatial distributions of red and blue points. A complication arises, however: the nature of the pattern depends on how the rat's location is defined. A rat is not a point object, and there is no single, obviously correct point on the rat's body to take as the "position" of the rat. In the current paradigm, different choices lead to different patterns. If we take the rat's position to be the location of the front LED array (which is usually about 5 cm in front of the rat's nose; see Figure 1), the pattern appears to be a diffuse blue core surrounded by a sharp red ring. If each point is shifted 9 cm back toward the rear LED (which corresponds to taking the rat's position to be approximately midway between the ears), then the pattern appears as a sharp red core surrounded by a diffuse blue ring.

The causes of these patterns are clarified by Figures 8C and D, of which C shows the same cell as Figure 8B, but broken down into data points at which the rat's head direction fell within four limited (90°) ranges of compass headings. It can be seen that the phenomenon is actually similar to that which occurs on a linear track: the earliest spikes, as the rat enters the place field, occur during the portion of the theta cycle extending from 60° before to 120° after the peak of pyramidal cell population activity (i.e., the blue points). Something more can be seen as well: the blue points are more broadly scattered than the red points. The latter effect appears more clearly in Figure 8D, which shows data from a different cell recorded at the same time; indeed most fields, when plotted in this way, are perceptibly more diffuse in the blue part of the theta cycle, but few show the effect as strongly as this one. (Note that Figures 8C and D are plotted using the recorded positions of the front LED, which, as illustrated in Figure 8B, actually maximizes the tightness of the blue points, not the red ones. If the points were all shifted 6–9 cm backward, the higher spatial specificity of the red points would become even more obvious.)

The consequence of these effects is that the pattern of activity must be described differently, depending on which part of the rat's body is chosen as the spatial location reference. If the front diode array is used, then the cell appears to fire only as the rat is moving away from the center of the place field, with blue spikes near the center and red spikes in a ring at the periphery. If the midpoint of the rat's ears is used, then the cell appears to fire only as the rat is moving toward the center of the place field, with blue spikes in a diffuse ring at the periphery and red spikes in a tight cluster at the center. If the rat's nose is used, then the cell appears

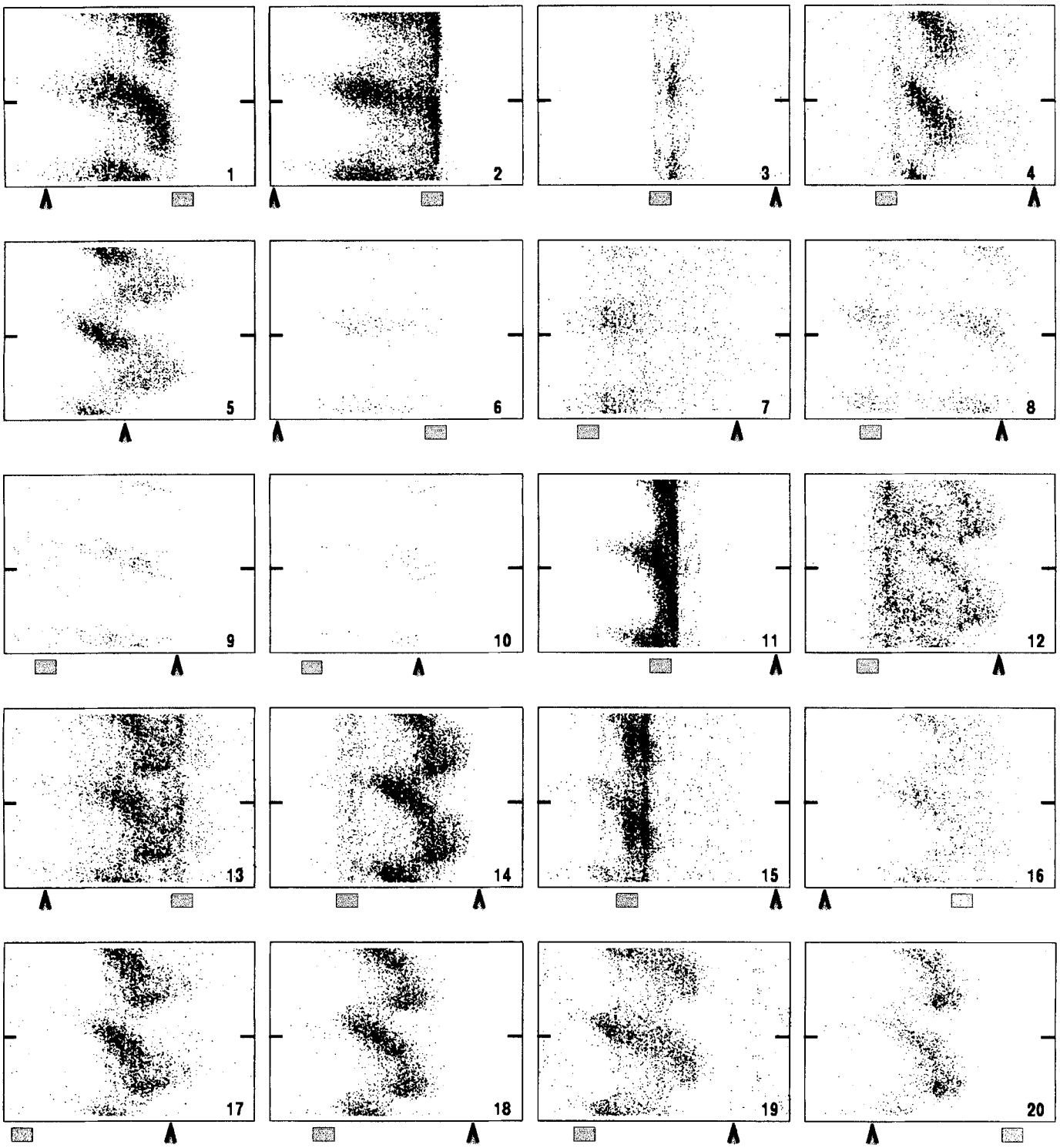

FIGURE 7. Plots of theta-modulated shifts in spatial firing, for 40 CA1 pyramidal cells recorded simultaneously on a triangle maze. Each plot shows data from a single cell; each point in the plot shows the location of the rat and the phase of the theta cycle at the moment a spike was emitted. To construct these plots, the triangle maze was "linearized" by projecting each recorded location to the nearest point on an equilateral triangle running down the center of the track, and then transforming this triangle into a line. The X axis represents the resulting point on this line, i.e., the rat's location on the maze; the Y axis represents theta phase. The range of X in each plot is 60 cm, which is slightly shorter than a single side of the triangle. The direction of motion is from left to right. The Y axis covers two full

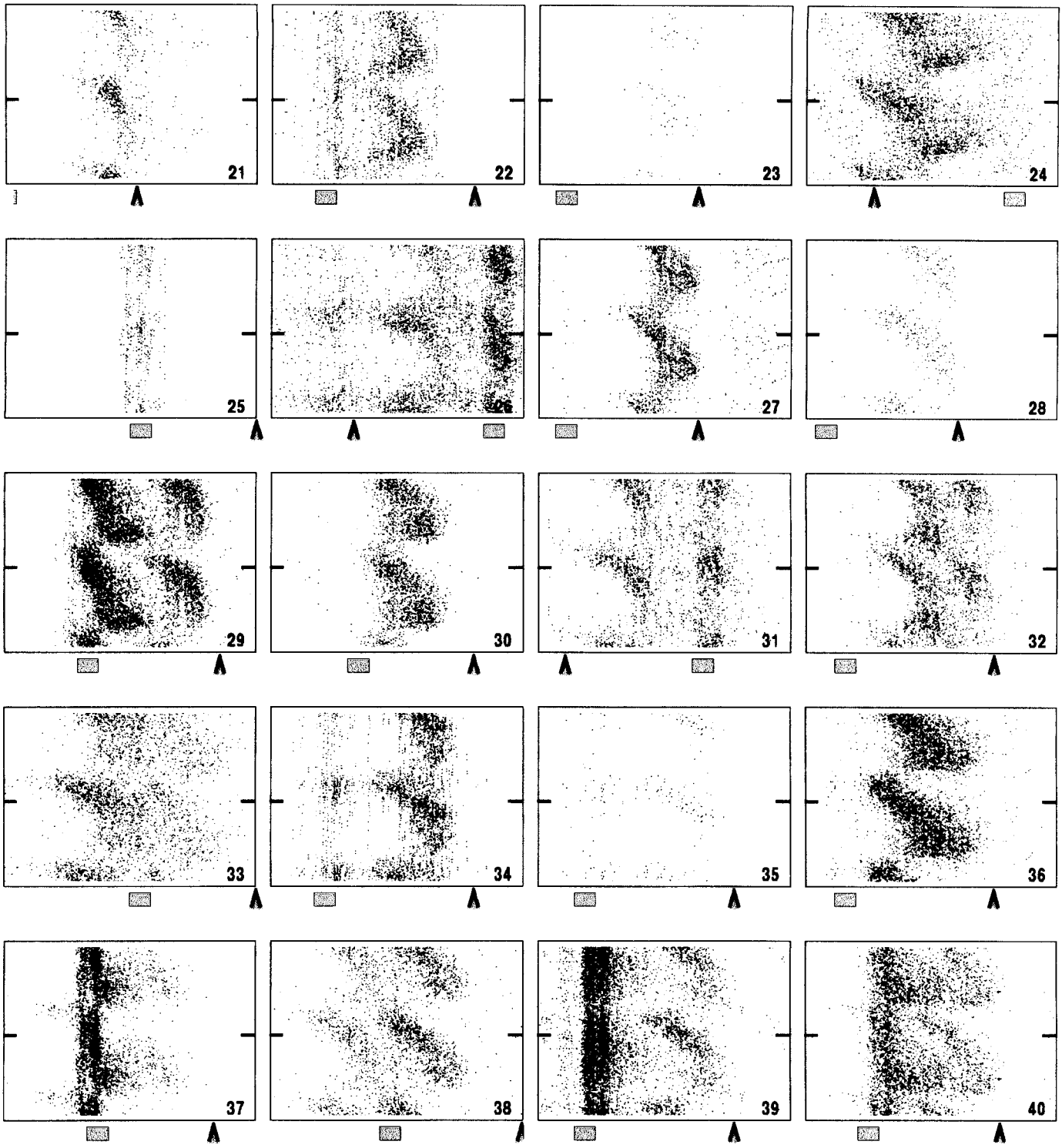

theta cycles, ranging from 0° at the bottom to 720° at the top, with the phase of maximum pyramidal cell population activity at the center (360°). Boxes below the plots mark food locations, where the rat usually stopped for a few seconds; arrows mark the corners of the triangle. The rat often turned its head from side to side while eating; this may in part account for the "smudgey" appearance of the firing patterns at the food locations. These data represent 55 min on the maze, and 131 circuits. Many other cells, recorded at the same time, were virtually silent on the maze, and are not shown.

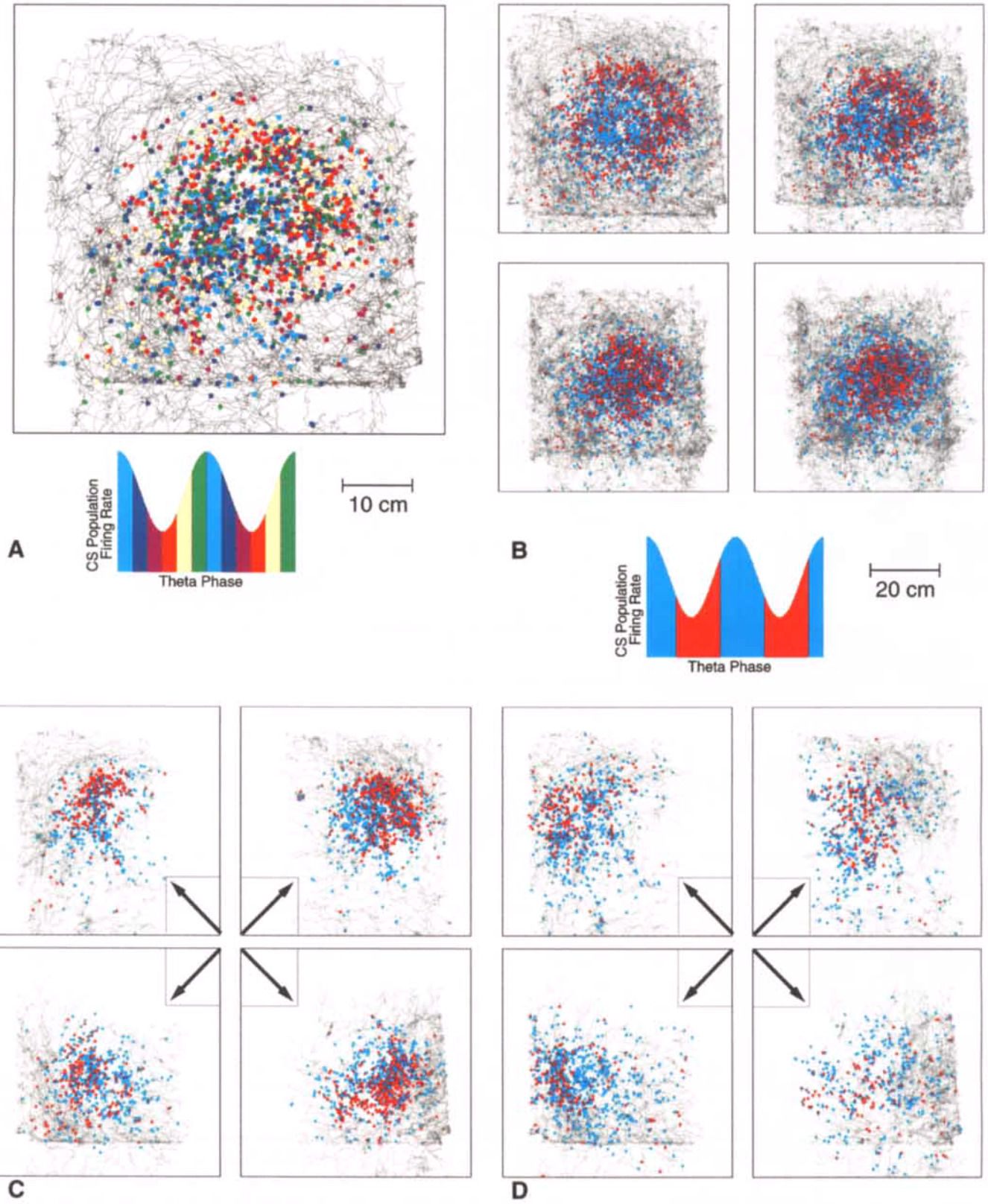
A
CS Population Firing Rate
Theta Phase
10 cm
B
CS Population Firing Rate
Theta Phase
20 cm
C
D

to fire both as the rat approaches and leaves the center of the place field, with blue spikes while he is approaching and red spikes while he is moving away. The reference point that leads to the tightest overall activity pattern is somewhere between the nose and eyes; the resolution of position tracking in these experiments does not permit greater precision.

To confirm the reality and consistency of the perceived differences in spatial tuning, we compared place fields for spikes occurring at different parts of the theta cycle, using three measures of spatial specificity, *information per spike*, *sparsity*, and *selectivity* (see Materials and Methods). For each cell, equal-sized samples of spikes were taken from the red and blue halves of the theta cycle, by randomly deleting spikes from the portion in which the cell was most active. Figure 9 shows scatterplots of the spatial specificity measures from three data sets, involving three different rats, two running in the apparatus from which the previous figures were drawn, and another in which the rat foraged for scattered food pellets on a rather narrow open rectangular platform. In each of these sets, the spatial specificity was significantly higher in the early (red) half of the theta cycle, on all measures ($P < 0.001$). The same test was performed on data taken from rats running on a triangular track, and a significant, but smaller, difference in spatial specificity was found in these circumstances as well. Figure 10 shows scatterplots of spatial specificity measures for three triangle maze data sets. In two of these data sets the information per spike is higher for the early half of the theta cycle, $P < 0.05$, and in one of the data sets the selectivity is significantly higher as well.

Granule Cells of the Fascia Dentata

The majority of granule cells isolated during sleep were virtually silent on the maze; but even for those that had place fields, the overall firing rates were usually quite low, commonly on the order of 0.5 Hz or less. Out of the 37 active granule cells that were recorded, three were exceptionally active, with mean firing rates of 2.95 Hz, 3.55 Hz, and 3.98 Hz on the triangle. One of these cells was examined in two separate environments and had a very strong place field in each; it also fired rather strongly during sleep. The other two cells had firing rates during sleep that fell within the range of variability of other putative granule cells. In spite of their unusually high firing rates, these three cells appeared in other ways similar to the other putative granule cells recorded here, showing the same patterns of phase precession and theta modulation.

Every dentate gyrus granule cell in the sample was strongly theta-modulated. Figure 11 shows theta tuning curves for a sample of 12 active granule cells. For most of them, peak firing occurred near phase 270°, with phase zero defined as the time of peak CA1 population activity. Also, most of these cells were very quiet near phase zero. A close examination indicates that the few exceptions (cells H, I, and J) showed a considerable amount of their activity while the rat was consuming the food reward at one of the goal locations. As illustrated in Figures 5D, 6, and 12, a robust pattern of phase precession could be seen in granule cells. It was not, however, the same as the pattern seen in CA1 pyramidal cells. In Figure 5, the difference manifests itself as an absence of blue points in the granule cell plot shown in panel D. For the CA1 pyramidal cells, blue-colored spikes were the first ones to appear as the rat enters the place field of a cell. This indicates that granule cells did not fire their first spikes in the same part of the theta cycle as did CA1 pyramidal cells, but rather about 90° earlier. Furthermore, the near-complete absence of blue points anywhere in Figure 5D indicates that this cell was nearly silent during the portion of the theta cycle in which CA1 pyramidal cells show their first spikes. The last spikes fired as the rat leaves a place field, for both types of cells, are colored red, indicating that the end-point of phase precession is the same for both types. As illustrated in Figure 12, these relationships held consistently for the granule cells in our sample.

FIGURE 8. Relations between theta phase and place-specific firing in a two-dimensional environment. A: Place field of a CA1 pyramidal cell, in a rat foraging for randomly scattered food pellets inside a square wooden box. (Refer to Figure 5 for the meaning of symbols and colors.) In this figure it is difficult to detect any relation between theta phase and spatial location; as the following figures show, such a relation is nevertheless present. B: Effect of varying the LED location upon the spatial pattern of firing for the cell shown in A, using a simplified color code. In the upper left panel each spike is plotted as a point at the location of the front LED array (i.e., 3–5 cm in front of the rat's nose) at the moment of the spike. In the next three panels the reference point for plotting spatial location is shifted respectively 3, 6, and 9 cm back toward the rear diode array, with the most posterior position corresponding approximately to the rat's ears or shoulders. The key describes the color code: blue corresponds to the half of the theta cycle beginning 60° before the peak of pyramidal cell population activity and ending 120° after the peak, red to the other half of the theta cycle. C,D: Spatial firing pattern for spikes occurring in different portions of the theta cycle, for two CA1 pyramidal cells (the first is the same cell shown in A and B). Each panel shows only samples during which the rat's head direction fell within a distinct 90° range of angles, indicated by the arrows. Thus, for example, the upper right panel shows all spikes and position points that occurred when the head direction fell between due north and due east.

Effect of Phase Precession on Spike Train Cross-Correlations

As pointed out in discussion by O'Keefe and Recce (1993), phase precession can be expected to affect the temporal relationships of spike activity for neurons with overlapping place fields, on a time scale shorter than the theta cycle. As Figure 14F explains, if a rat passes sequentially through two adjoining place fields, the first cell will fire early in the theta cycle while the second cell fires late in the theta cycle. This prediction is confirmed by an examination of cross-correlation histograms. Figure 13 shows a spatial firing map for four CA1 pyramidal cells with nearby place fields on the triangle maze, together with their cross-correlation histograms. Strong theta modulation can be seen in each histogram, and in each case, the peak closest to zero is shifted away from zero, in the direction matching the order in which the rat traverses the two place fields. Moreover, the amount of peak shift is approximately proportional to the distance by which the

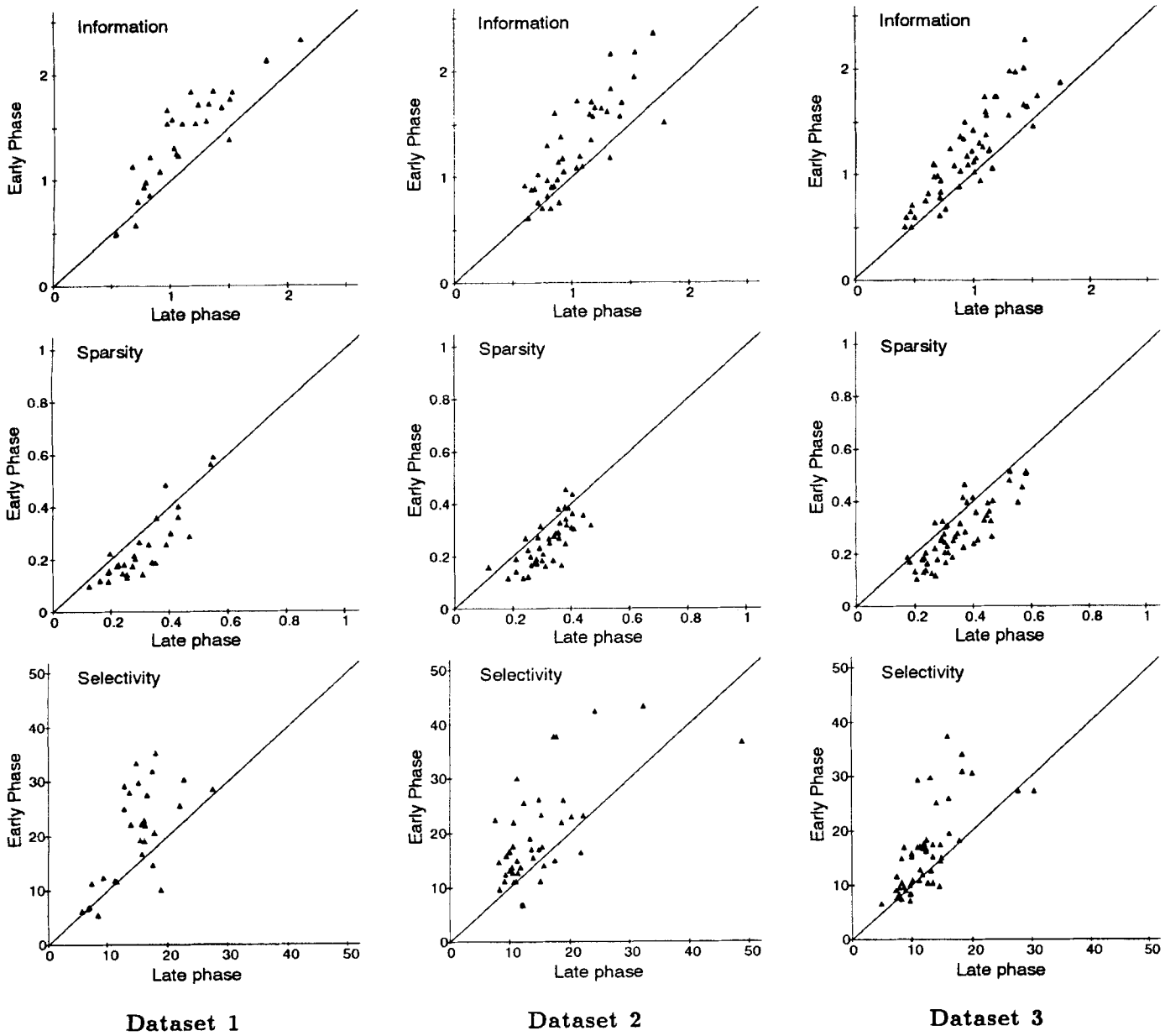

FIGURE 9. Scatterplots of spatial specificity measures for activity during the early and late portions of the theta cycle (as defined for Figure 8), for three rats foraging for food reward in a rectangular region. Each plot shows data taken from a single rat, in a single recording session. Each plot is calculated on the basis of spikes occurring while the rat faced into a 90° range of head directions, with the X coordinate representing the late phase and the Y coordinate the early phase. The fact that most of the points lie above the main diagonal for the information measure, below the main diagonal for the sparsity measure, and above the main diagonal for the selectivity measure, indicates that firing is more spatially specific in the early portion of the theta cycle than in the late portion. All differences are significant, $P < 0.001$ (Student's t-test, two-tailed).

two place fields are separated. These relations held for every pair of cells we have examined with overlapping place fields on the triangular track.

DISCUSSION

The foregoing results clarify the relationship between the hippocampal theta rhythm and the spatial firing of hippocampal cells, by establishing that:

1. On linear tracks, the tendency of spikes to shift to earlier theta phases, described first by O'Keefe and Recce (1993), can be seen in almost every active CA1 pyramidal cell. Phase precession is probably not caused by an activity-dependent mechanism within individual CA1 pyramidal cells, because there are many examples of low-rate cells that exhibit the same rate and range of precession as high-rate cells. Phase precession can also be seen in two-dimensional environments, where the animal is not constrained to travel along stereotyped trajectories, but it does not appear to be as robust under these conditions.

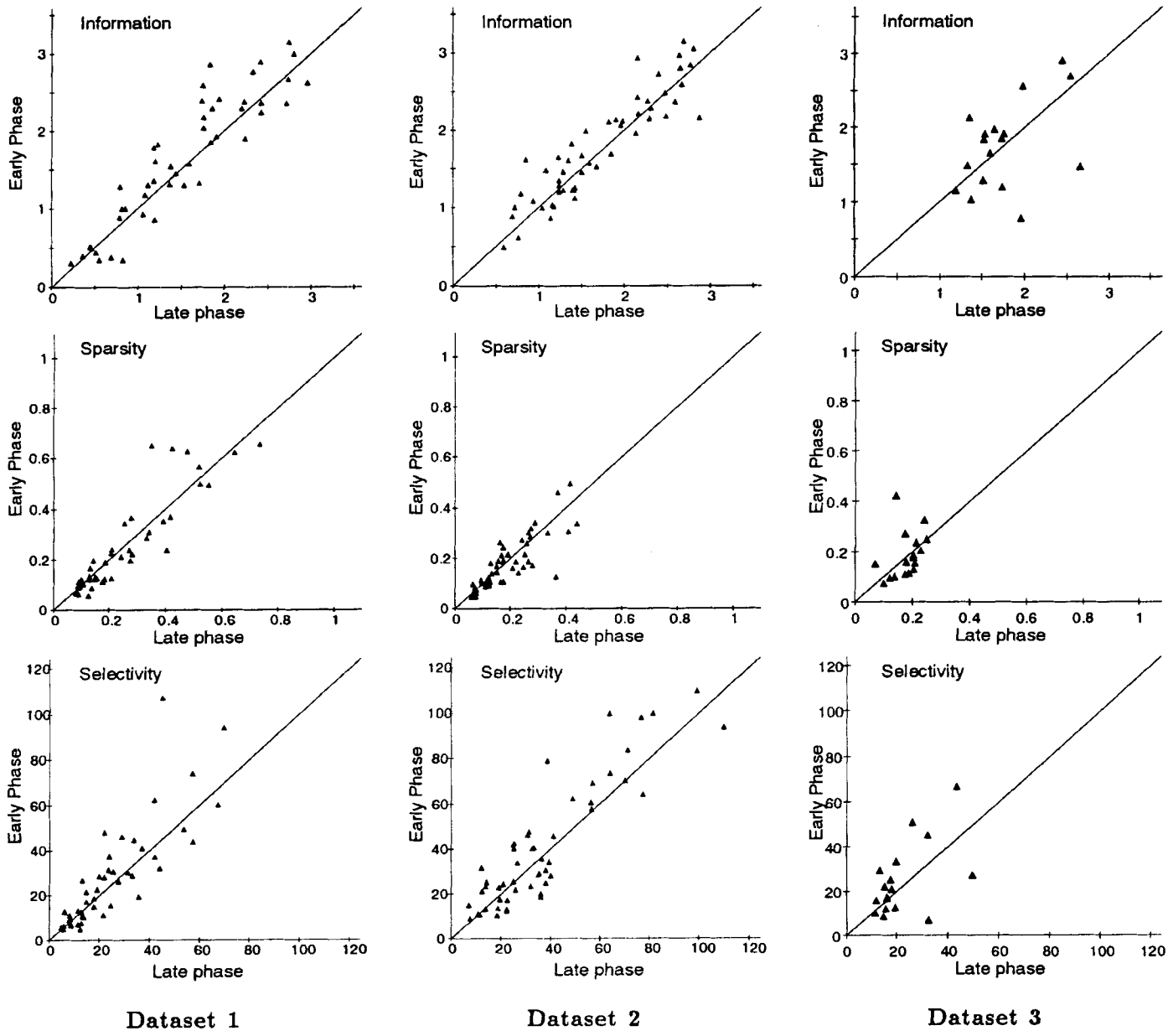

FIGURE 10. Scatterplots of spatial specificity measures for activity during the early and late portions of the theta cycle, for three rats running for food reward on a triangular track. The differences in information per spike for data sets 1 and 2 are significant, $P < 0.05$, as is the difference in selectivity for data set 1, $P < 0.05$.

2. Every cell shows its first activity, as the rat enters the cell's place field, approximately 90°–120° after the phase corresponding to peak CA1 pyramidal cell population activity, at about the phase where total inhibitory activity is least. As O'Keefe and Recce (1993) reported, for many cells the firing precesses through almost a full 360°. Thus CA1 pyramidal cells show coherent phase precession, as defined in the introduction to this paper. This finding demarcates a specific phase of the theta cycle at which the pattern of population activity changes in a very abrupt, almost discontinuous, manner. It is natural to define this phase as the beginning/end of the theta cycle (we have already been using this terminology); it falls approximately 90° after the peaks of EEG theta waves recorded at the depth of the hippocampal fissure.

3. In two-dimensional environments, CA1 pyramidal cell firing shows considerably sharper spatial specificity during the early portion of the theta cycle than during the later portion. This difference cannot be accounted for merely by the difference in overall firing rates between the early and late portions of the theta cycle. A difference in the same direction, but smaller in magnitude, is seen on a linear track.

4. The activity of granule cells of the fascia dentata is strongly modulated by the theta rhythm. This should be considered a novel finding (though not unexpected), because previous analyses of granule cells have been based on the assumption that they are "theta cells" with high firing rates. The current data indicate that peak granule cell population activity precedes peak CA1 pyrami-

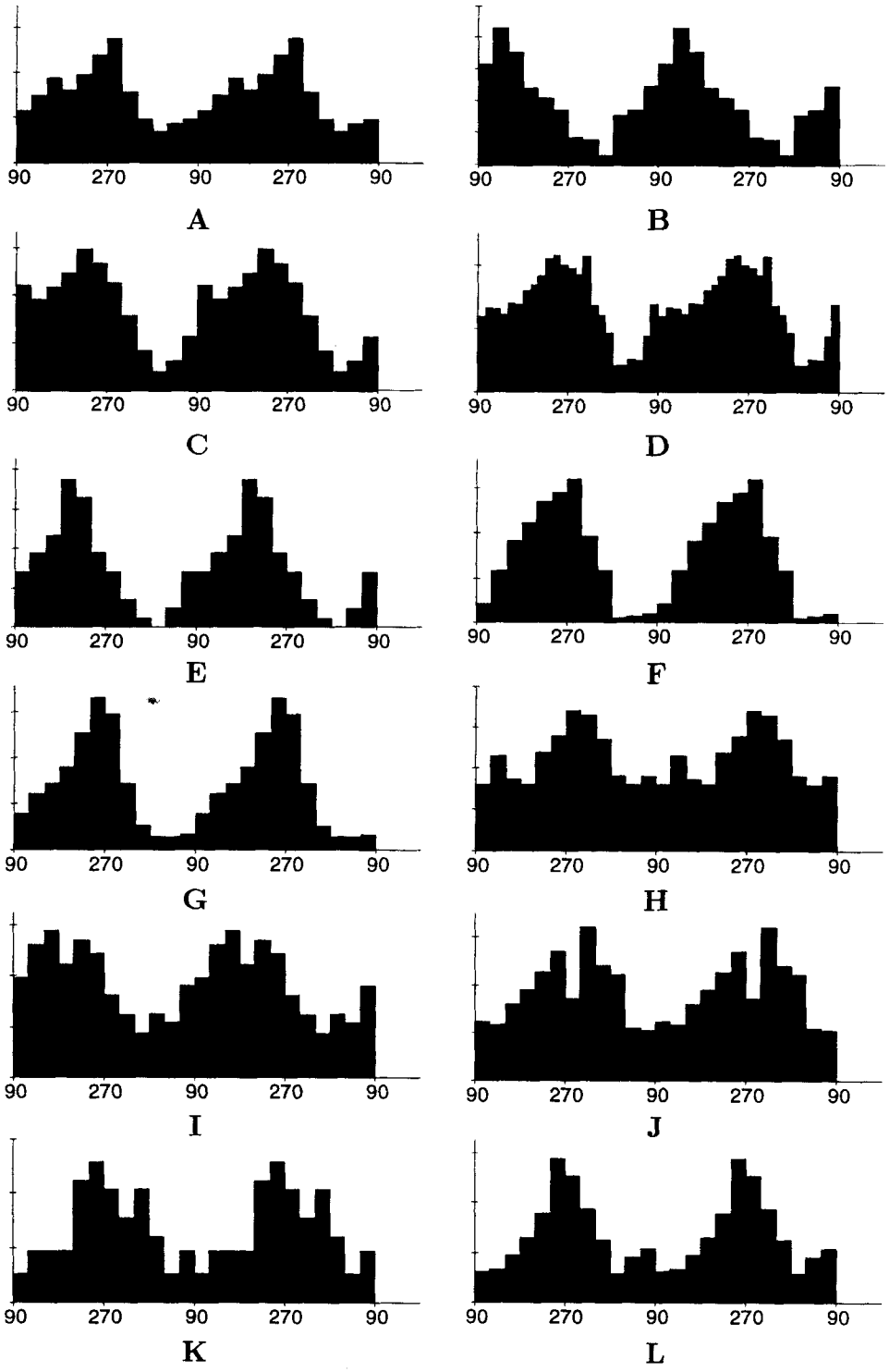

FIGURE 11. Firing rates of 12 putative dentate gyrus granule cells, as a function of phase of the theta cycle. Mean firing rates: A, 0.54 Hz; B, 0.20 Hz; C, 0.51 Hz; D, 0.19 Hz; E, 0.17 Hz; F, 0.30 Hz; G, 0.78 Hz; H, 0.56 Hz; I, 0.94 Hz; J, 0.45 Hz; K, 0.22 Hz; L, 1.12 Hz. All of these cells had tight place fields, inside which the firing rates were much higher; the maximum was 47.1 Hz at the center of the place field, for cell C. The fields for cells B, H, I, and J were at reward locations, where the rat spent much of the time either consuming food or turning his head from side to side.

dal cell population activity by about 90°, and that granule cells as a population are much more deeply modulated than CA1 pyramidal cells, being very quiet during the last quarter of the theta cycle.

5. Dentate gyrus granule cells show robust phase precession on a linear track. Their first spikes come about 90° earlier in the theta cycle than the first spikes for CA1 pyramidal cells; the last spikes for both types of cells come near the beginning of the theta cycle.

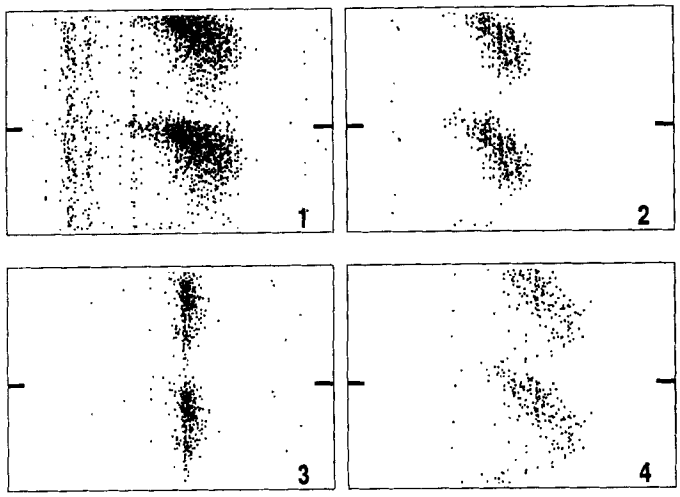

FIGURE 12. Plots of the relation of theta phase and spatial location for spike activity from four dentate gyrus granule cells. Refer to Figure 7 for explanation of the plots. Note that for each of these cells, the first spikes, as the rat enters the place field, occur at approximately the phase of maximal CA1 population activity, i.e., approximately at the same level as the horizontal ticks. This is about 90° earlier in the theta cycle than the first spikes for the CA1 pyramidal cells shown in Figure 7. Note also that each of the four cells shows very little spike activity during the 90° interval following the tick marks.

The pattern of activity as a rat passes through a strong place field in a specific direction resembles the schema of Figures 14B and C. If the rat passes through the center of the place field, strong phase precession is seen, with the spikes precessing, in an accelerating manner, from the end to the beginning of the theta cycle. If the rat skirts the edge of the place field, the first spikes still occur at the end of the theta cycle, but there may be only a partial phase precession. This qualitative pattern is seen both in one- and two-dimensional environments, but there appear to be quantitative differences. In two-dimensional environments, spike activity shows a relatively weaker phase advance, and a relatively stronger change in spatial specificity, than in one-dimensional environments.

For multidirectional place fields, the correct way to describe the spatial firing pattern is not entirely clear, because it depends on which part of the animal's body is taken to represent its spatial location (Fig. 14E). Without a principled way of resolving this ambiguity, it seems impossible to say whether cells begin firing in the periphery of the field and cease firing in the center, or begin near the center and cease in the periphery, or something else. This uncertainty makes it difficult to determine what is represented by each phase of the theta cycle. Does the last part of the cycle represent memory, or does the first part represent anticipation, or both, or neither? These questions cannot currently be answered with any confidence.

The present data are in agreement with earlier reports that CA1 pyramidal cells fire maximally near the positive peak of the EEG theta waves at the level of the dentate gyrus molecular layer (Buzsáki et al., 1993; Fox et al., 1986); there is, though, some variability, probably related to the way the animal behaves inside the place field. Our data further indicate that the depth of modulation for the CA1 pyramidal cell population is on the order of 50%. This value, however, results from two separate factors. The first is that the depth of modulation, averaged across many cells and/or cycles, contains a blurring effect due to the precession of firing. In addition, there is an increase in phase dispersion, as a function of position, such that near the center of a place field there is often significant firing throughout the cycle. The true cycle-to-cycle depth of modulation for individual cells is greater than 90% (Fig. 6). Theta cells, on the other hand, are highly variable in their tuning to the theta rhythm, in terms of both depth of modulation and the phase corresponding to maximal firing. It appears that the overall level of inhibition is likely to be minimal 90°–120° after the peak of pyramidal cell population activity, but this requires further investigation. The present data also indicate that granule cells of the fascia dentata are phase-advanced by about 90° with respect to CA1 pyramidal cells. It is interesting to note that Buzsáki et al. (1983) found the same relationship for theta EEG waves recorded in the fascia dentata and in CA1. As a matter of fact, they anticipated the present finding that granule cells precede CA1 pyramidal cells by about 90°, but the cells they identified as granule cells would have been classified by us as interneurons. (Many of the interneurons we encountered in the fascia dentate showed peak activity at approximately the same theta phase as the granule cell population.)

The physiological mechanisms responsible for phase precession remain unclear. O'Keefe and Recce (1993) suggested that the phase shift is produced by an interaction between extrinsic theta-frequency modulation of pyramidal cells, and an intrinsic tendency of these cells to oscillate at a slightly higher frequency. The data presented in this paper raise the alternative possibility that the phase shift in CA1 could be inherited from the fascia dentata or an earlier stage of the hippocampal circuit.

It is important to understand how such inheritance could occur. Suppose there are two brain areas, X and Y, with Y receiving much of its input from X, so that the pattern of activity in Y is largely determined by the pattern of activity in X; let us say that a pattern A in X gives rise to a pattern A′ in Y. Suppose now that area X encodes a representation of spatial location, and that the animal passes through a sequences of places represented by A,B,C,D,E. As illustrated in Figure 14F, a phase precession effect in area X would cause the temporal pattern of activity there to be something like

$$\ldots |ABC|ABC|BCD|BCD|CDE|CDE| \ldots,$$

where the vertical bars represent the beginning/end of the theta cycle. If the corresponding patterns induced in area Y are $A \rightarrow A'$, $B \rightarrow B'$, $C \rightarrow C'$, $D \rightarrow D'$, $E \rightarrow E'$, then the resulting temporal pattern of activity in area Y will be

$$\ldots |A'B'C'|A'B'C'|B'C'D'|B'C'D'|C'D'E'|C'D'E'| \ldots.$$

Thus, area Y effectively inherits the phase precession effect from area X. It can be seen from this argument that two things are necessary for inheritance to take place: 1) the projection from X to Y must be strong enough for the activity pattern in X to deter-

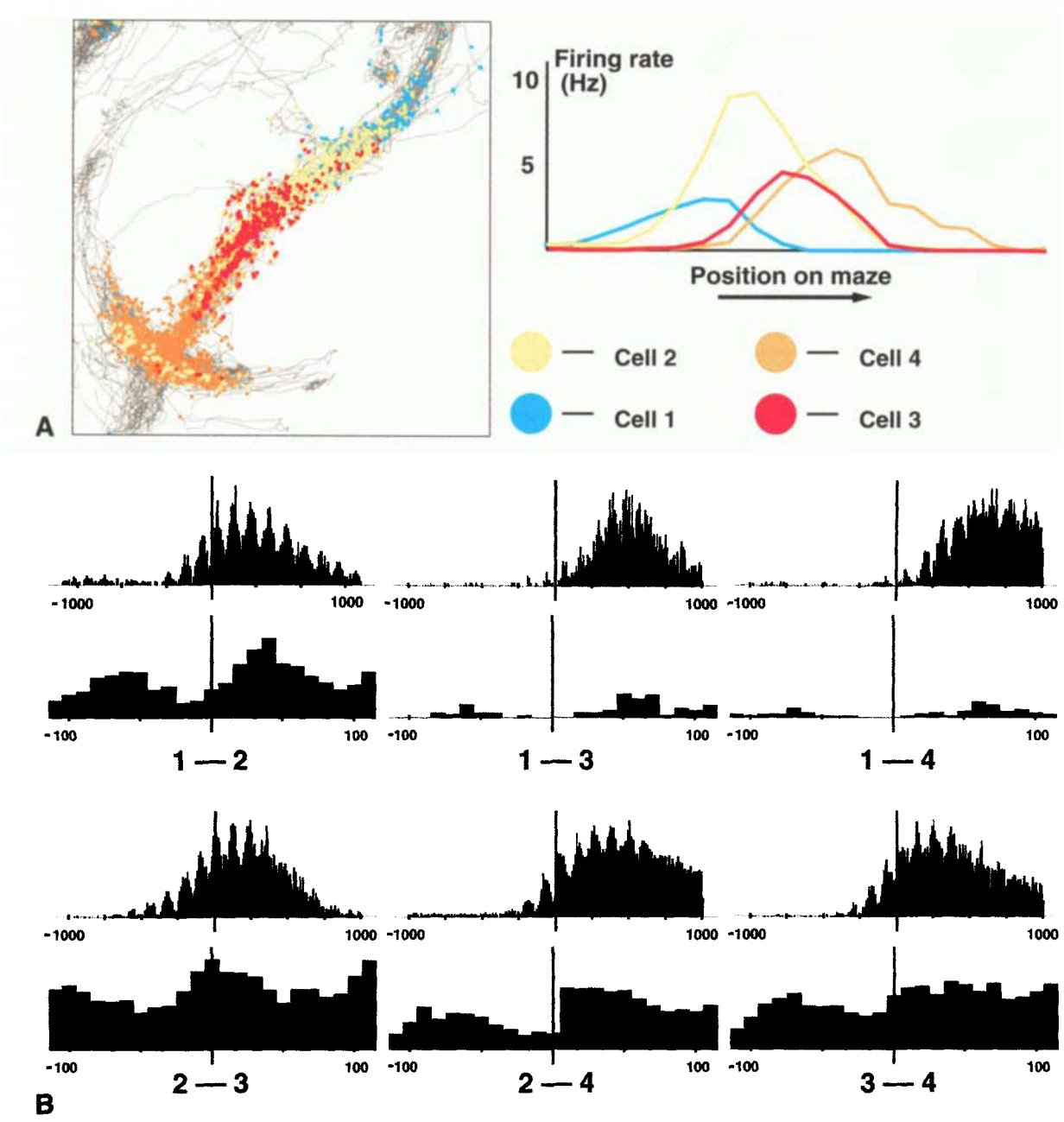

FIGURE 13. Cross-correlation histograms for four CA1 pyramidal cells with neighboring place fields on the triangle maze. A, left: Spatial firing map for the four cells, following the scheme of Figure 5. The direction of motion is from upper right to lower left; one of the three reward locations can be seen in the lower left corner. A, right: Plot of spatial mean firing rates for the four cells, as a function of position on the maze. The direction of motion is from left to right. B: Cross-correlation histograms for each pair of the cells, over two time ranges. The top histogram of each pair shows a 1 s (= 1,000 ms) time window, the bottom a 100 ms time window. The bin size for all histograms is 10 ms. Each bar represents the total number of instances in which a spike of the first cell was followed at latency X by a spike of the second cell, possibly with other spikes in between. Because the cells are ordered according to the sequence in which the rat passed through their place fields, the top histograms are all peaked to the right of the origin; all of them show strong theta modulation. The lower histograms (which are merely an expansion of the central region of the upper ones) demonstrate that the theta-frequency peaks are also shifted to the right from the origin, by an amount that depends on the distance between the place fields. Thus there is a consistent relation between the sequence in which the place fields are traversed and the shift of the cross-correlation peak nearest to the origin: this is a consequence of phase precession.

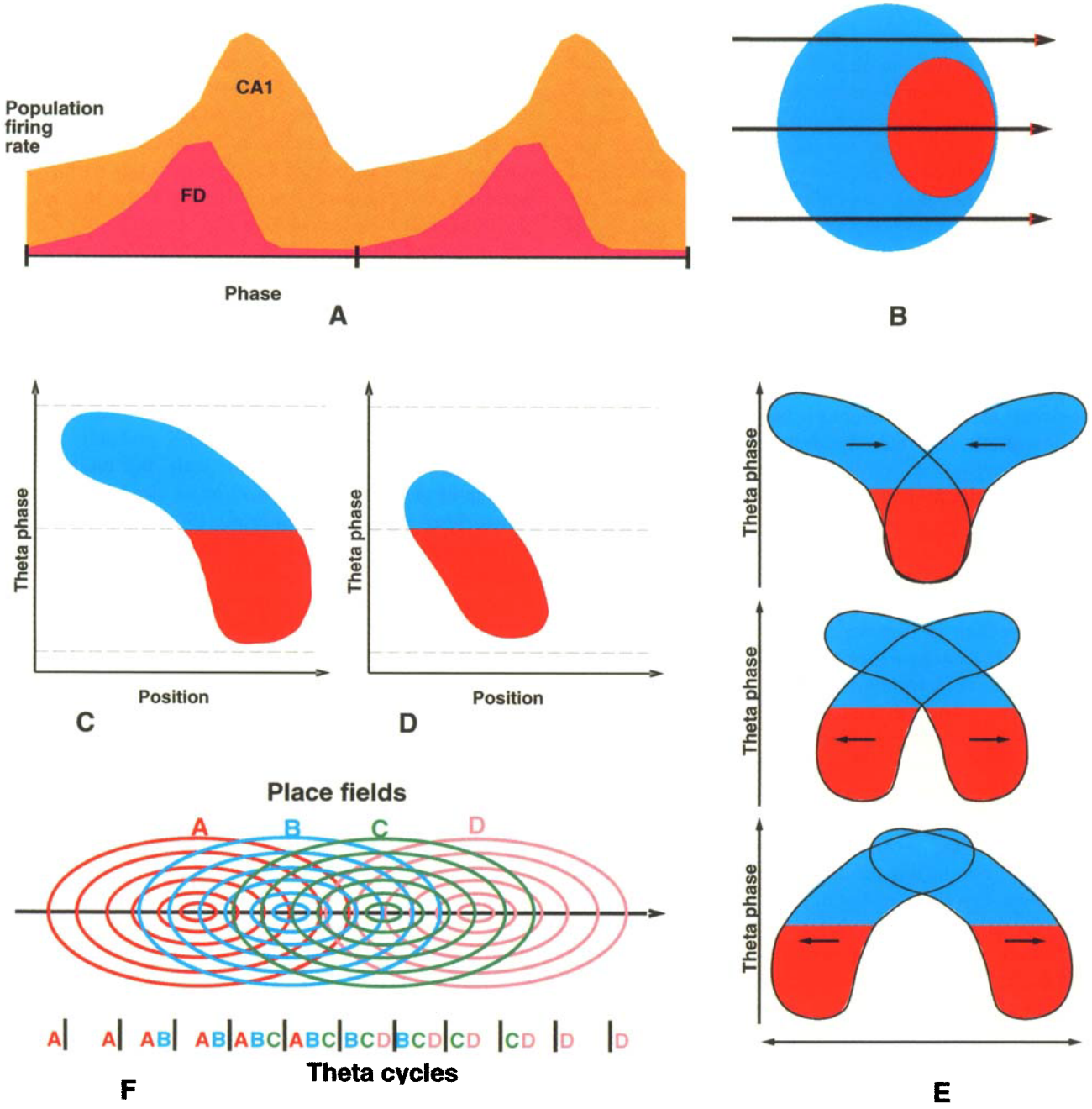

FIGURE 14. Summary of results. (Each part of this figure was drawn by hand.) A: Population firing rates of CA1 pyramidal cells and dentate gyrus granule cells, as a function of theta phase. CA1 pyramidal cell population activity is modulated by about 50%, and peaks about 90° before the end of the theta cycle. Granule cells fire at lower average rates, are modulated much more strongly, and show peak population activity near the middle of the theta cycle, about 90° in advance of CA1 pyramidal cells. B: Relation between theta phase and spatial firing in a two-dimensional environment, for a CA1 pyramidal cell. Red indicates spikes occurring in the first half of the theta cycle, blue spikes occurring in the second half. Arrows indicates the rat's direction of motion. When the rat passes through the center of the place field, blue spikes occur first, followed by red spikes. When the rat passes through the periphery of the place field, off to one side of the center, only blue spikes occur. Thus the red spikes are more tightly concentrated in space than the blue spikes. C: Relation between theta phase and spatial firing for a CA1 pyramidal cell. The X axis represents the rat's location, with the direction of motion going from left to right; the Y axis represents phase of the theta cycle, with the interval between dotted lines equal to 180°. The activity shifts, in an accelerating manner, from blue to red as the rat passes through the place field. D: Relation between theta phase and spatial firing for a granule cell of the fascia dentata. The cell is nearly silent for the last quarter of the theta cycle, but otherwise shows phase precession similar to that seen in CA1. E: Ambiguity in the perceived relationship between theta phase and spatial location, for a cell that fires during passes through a particular location in diametrically opposite directions. During passes in each direction individually, the pattern is identical to the one shown in panel C, but the way the two directions combine depends on which point on the rat's body is used to determine its position. If the reference point is near the back of the rat's head, the overall pattern appears as a tight red center with a diffuse blue surround (top). If the reference is near the rat's nose, the pattern appears as a diffuse blue center with a red surround (bottom). If the reference is near the rat's eyes, the pattern consists of red and blue thoroughly intermingled (center). F: Phase precession leads to compressed representation of temporal structure within single theta cycles. The picture illustrates what happens when the rat passes through four partially overlapping place fields A, B, C, D. Below, spikes from each cell are shown precessing gradually from the end to the beginning of the theta cycle. Consequently, portions of the sequence ABCD are replicated repeatedly within individual theta cycles.

mine the activity pattern in Y; and 2) the synaptic integration time scale in area Y must be much shorter than the theta cycle. If (1) does not occur, that is, if the projection from X to Y is relatively weak, then area Y may not inherit a full scale phase precession, but some degree of phase-position interaction in area Y can still be predicted. If (2) does not occur, then the phase precession could be "averaged out" in area Y. In the hippocampus, most of the principal excitatory pathways involve glutamate impinging on AMPA receptors. These receptors have time constants of less than 5 ms, and the membrane time constants of the neurons are probably considerably less than 20 ms in natural conditions (with a constant background of $GABA_a$-mediated inhibition impinging on the soma), so the time constant of integration for most areas in the hippocampus is likely to be at least an order of magnitude less than the duration of the theta cycle. Therefore "averaging out" of phase precession is unlikely to occur. The status of requirement (1) in the hippocampus is not as clear. CA1 receives a very strong input from CA3 via the Schaffer collaterals, but it also receives a substantial input from the entorhinal cortex, so it is unlikely that CA3 has complete control over the pattern of activity in CA1. Similarly, CA3 receives important inputs both from mossy fibers arising in the fascia dentata and directly from perforant path inputs.

The hypothesis of inheritance of phase precession merely shifts the issue of its mechanism to an earlier processing stage. One model that has recently been proposed is that the precession effect arises as a consequence of periodic gating of input to the hippocampus in conjunction with an asymmetry in the intrinsic connections (Tsodyks et al., 1996). According to this hypothesis, the state of the network is set at the beginning of each cycle by the extrinsic input, but the internal dynamics then cause the network to advance through the sequence of states along the trajectory at a rate that is much faster than the actual motion of the rat.

The functional role of phase precession is also at present unclear, if indeed there is one. Burgess et al. (1994) developed a neural network model of spatial navigation, in which phase precession serves to link the rat's location with a goal location lying in front of or behind it. The data from our experiments appear to be entirely consistent with the requirements of the Burgess et al. model, and are also consistent with data briefly presented in their paper regarding the correlates of theta phase in the open field.

We would like to propose, though, that the influence of phase precession on cross-correlations raises an alternative possibility. An inevitable consequence of the phase shift is that, when the rat passes through a sequence of place fields, portions of this sequence will be replicated, in compressed form, within individual theta cycles (Fig. 14F). Moreover, each portion of the sequence is repeated several times as the rat moves along. To clarify this, let us suppose that each cell represents a specific point in space, and imagine that we "reconstruct" the location represented by the CA1 population (as done by Wilson and McNaughton, 1993), on the basis of very brief (say, 5 ms) samples of population activity. The data predict that during each theta cycle, the reconstructed location will shift forward along the rat's trajectory, for a net distance approximately the size of one average place field.

We propose that this compression and repetition of neural activity sequences may make it possible to use long-term potentiation (LTP) to memorize the temporal structure of the rat's experience. Due to the properties of the NMDA receptor, LTP is probably capable of making associations across a time span approaching, but not much longer than, 50 ms, which is less than the duration of a theta cycle (Levy and Steward, 1983; Gustaffson and Wigström, 1986; Larson and Lynch, 1989). This time range results from the fact that inflow of calcium through the NMDA receptor occurs whenever there is a conjunction of two circumstances (Brown et al., 1991): 1) glutamate must be bound to the NMDA receptor, in order to open the channel, and 2) the postsynaptic cell membrane must be depolarized, in order to remove magnesium that otherwise clogs the open channel. Movement of magnesium in and out of the channel probably occurs very rapidly, on a sub-millisecond time scale, but binding and unbinding of glutamate occurs much more slowly, on a time scale approaching 100 ms (Brown et al., 1991). The consequence of these factors is that, in order to achieve the necessary conjunction, presynaptic glutamate release must occur *before* postsynaptic depolarization, and it may in principle occur as much as 100 ms before. These theoretical predictions have to some extent been experimentally confirmed: experiments performed by Levy and Steward (1983) and by Gustaffson and Wigström (1986) have demonstrated that LTP may be achieved when the presynaptic fibers are stimulated as much as 40 ms before postsynaptic depolarization is induced. If the order is reversed, no potentiation is seen. Additional support is provided by results of Larson and Lynch (1989), who showed that the sequence in which a set of afferents to CA1 are stimulated determines the degree to which they potentiate; the first and last elements of the sequence were separated by 70 ms.

As pointed out in this paper, phase precession causes a substantial asymmetry in the cross-correlation of pairs of units within a time window of 50–100 ms around the origin. Moreover, the asymmetry always leads to a peak shift in the direction matching the order in which the two cells are activated by the rat's behavior on the maze. The prediction, then, is that this asymmetry will lead to asymmetrical potentiation of the connections between the two cells.

Thus, compression of sequences could serve to bring the temporal structure within the span of LTP, while repetition could afford opportunities to cement each association (cf. Granger et al., 1994). The most critical requirement is that LTP be especially favored when presynaptic activity occurs earlier in the theta cycle than postsynaptic activity. The available data are generally consistent with this prediction (e.g., Pavlides, 1988; Greenstein, 1988; Diamond et al., 1988; Robinson, 1986; Otto et al., 1991), but further investigation is needed. The proposed mechanism could not subsist in CA1 alone, because of the dearth of recurrent connections there, but if, as now seems likely, phase precession also occurs in CA3, then the mechanism could apply both to the recurrent collaterals within CA3 and the Schaffer collateral projections from CA3 to CA1.

A strong case can be made that the hippocampus is essential for episodic/declarative memory (Tulving, 1972; Squire, 1992;

Cohen and Eichenbaum, 1993), a central feature of which is the preservation of temporal order; indeed, recent experiments in this laboratory confirm that the hippocampus retains information about the order in which neurons fire in an environment (Skaggs and McNaughton, 1996). If the theta rhythm creates the capacity for hippocampal memory for temporal sequences, this may be an important enough function to explain why the rhythm exists.

Acknowledgments

We thank John O'Keefe, Gyuri Buzsáki, Arthur Winfree, Misha Tsodyks, Mayank Mehta, Jim Knierim, and Alexei Samsonovich for helpful discussions; Kevin Moore, Rowena D'Monte, and Matt Suster for assistance with data acquisition; Michael Williams for technical support; and Keith Stengel for engineering development of the parallel recording apparatus. Supported by MH 46823 and O.N.R.

REFERENCES

Artemenko DP (1973) Participation of hippocampal neurons in theta-waves generation. Neurophysiology 4:409–415.

Barnes CA, McNaughton BL, O'Keefe J (1983) Loss of place specificity in hippocampal complex spike cells of senescent rat. Neurobiol Aging 4:113–119.

Bland BH (1986) The physiology and pharmacology of hippocampal formation theta rhythms. Prog Neurobiol 26:1–54.

Bland BH, Colom LV (1993) Extrinsic and intrinsic properties underlying oscillation and synchrony in limbic cortex. Prog Neurobiol 41:157–208.

Brown TH, Zador AM, Mainen ZF, Claiborne BJ (1991) Hebbian modifications in hippocampal neurons. In: Long-term potentiation: A debate of current issues (Baudry M, Davis JL, eds), pp 357–389. Cambridge, Massachusetts: MIT Press.

Buño W, Velluti JC (1977) Relationships of hippocampal theta cycles with bar pressing during self-stimulation. Physiol Behav 19:615–621.

Burgess N, Recce M, O'Keefe J (1994) A model of hippocampal function. Neural Networks 7:1065–1081.

Buzsáki G, Leung LS, Vanderwolf CH (1983) Cellular bases of hippocampal EEG in the behaving rat. Brain Res Rev 6:139–171.

Buzsáki G, Czopf J, Kondakor I, Kellenyi L (1986) Laminar distribution of hippocampal rhythmic slow activity (RSA) in the behaving rat: Current-source density analysis, effects of urethane and atropine. Brain Res 365:125–137.

Buzsáki G, Horvath Z, Urioste R, Hetke J, Wise K (1992) High-frequency network oscillation in the hippocampus. Science 256:1025–1027.

Cohen NJ, Eichenbaum H (1993) Memory, amnesia, and the hippocampal system. Cambridge, MA: MIT Press.

Diamond DM, Dunwiddie TV, Rose GM (1988) Characteristics of hippocampal primed burst potentiation in vitro and in the awake rat. J Neurosci 8:4079–4088.

Eichenbaum H, Wiener SI, Shapiro ML, Cohen NJ (1989) The organization of spatial coding in the hippocampus: A study of neural ensemble activity. J Neurosci 9:2764–2775.

Fox S, Ranck JB Jr (1981) Electrophysiological characteristics of hippocampal complex-spike cells and theta cells. Exp Brain Res 41:399–410.

Fox SE, Wolfson S, Ranck JB Jr (1986) Hippocampal theta rhythm and the firing of neurons in walking and urethane anesthetized rats. Exp Brain Res 62:495–508.

Fujita Y, Sato T (1964) Intracellular records from hippocampal pyramidal cells in rabbit during theta rhythm activity. J Neurophysiol 27:1011–1025.

Granger R, Whitson J, Larson J, Lynch G (1994) Non-Hebbian properties of long-term potentiation enable high-capacity encoding of temporal sequences. Proc Natl Acad Sci USA 91:10104–10108.

Green JD, Arduini A (1954) Hippocampal electrical activity in arousal. J Neurophysiol 17:533–557.

Greenstein YJ, Pavlides C, Winson J (1988) Long-term potentiation in the dentate gyrus is preferentially induced at theta rhythm periodicity. Brain Res 438:331–334.

Gustaffson B, Wigström H (1986) Hippocampal long-lasting potentiation produced by pairing single volleys and brief conditioning tetani evoked in separate afferents. J Neurosci 6:1575–1582.

Jung R, Kornmüller AE (1938) Eine Methodik der Ableitung lokalisierter Potentialschwankungen aus subcorticalen Hirngebieten. Arch Psychiat Nervenkr 109:1–30.

Jung MW, McNaughton BL (1993) Spatial selectivity of unit activity in the hippocampal granular layer. Hippocampus 3:165–182.

Kramis R, Vanderwolf CH, Bland BH (1975) Two types of hippocampal rhythmical slow activity in both the rabbit and the rat: Relations to behavior and effects of atropine, diethyl ether, urethane, and pentobarbital. Exp Neurol 49:58–85.

Larson J, Lynch G (1989) Theta pattern stimulation and the induction of LTP: The sequence in which synapses are stimulated determines the degree to which they potentiate. Brain Res 489:49–58.

Leonard B (1990) The contribution of velocity, spatial experience, and proximal visual complexity to the location- and direction-specific discharge of hippocampal complex-spike cells in the rat. PhD thesis, University of Colorado, Boulder, CO.

Leung LS (1984) Model of gradual phase shift of theta rhythm in the rat. J Neurophysiol 52:1051–1065.

Levy WB, Steward O (1983) Temporal contiguity requirements for long-term associative potentiation/depression in the hippocampus. Neuroscience 8:791–797.

Macrides F, Eichenbaum H, Forbes WB (1982) Temporal relationship between sniffing and the limbic theta rhythm during odor discrimination reversal learning. J Neurosci 2:1705–1717.

McNaughton BL, Barnes CA, O'Keefe J (1983a) The contributions of position, direction, and velocity to single unit activity in the hippocampus of freely-moving rats. Exp Brain Res 52:41–49.

McNaughton BL, O'Keefe J, Barnes CA (1983b) The stereotrode: A new technique for simultaneous isolation of several single units in the central nervous system from multiple unit records. J Neurosci Methods 8:391–397.

McNaughton BL, Barnes CA, Meltzer J, Sutherland RJ (1989) Hippocampal granule cells are necessary for normal spatial learning but not for spatially selective pyramidal cell discharge. Exp Brain Res 76:485–496.

Muller RU, Kubie JL, Ranck JB (1987) Spatial firing patterns of hippocampal complex-spike cells in a fixed environment. J Neurosci 7:1935–1950.

O'Keefe J (1976) Place units in the hippocampus of the freely moving rat. Exp Neurol 51:78–109.

O'Keefe J, Conway DH (1978) Hippocampal place units in the freely moving rat: why they fire where they fire. Exp Brain Res 31:573–590.

O'Keefe J, Dostrovsky J (1971) The hippocampus as a spatial map. Preliminary evidence from unit activity in the freely moving rat. Brain Res 34:171–175.

O'Keefe J, Nadel L (1978) The hippocampus as a cognitive map. Oxford: Clarendon Press.

O'Keefe J, Recce ML (1993) Phase relationship between hippocampal place units and the EEG theta rhythm. Hippocampus 3:317–330.

Olton DS, Branch M, Best PJ (1978) Spatial correlates of hippocampal activity. Exp Neurol 58:387–409.

Otto T, Eichenbaum H, Wiener SI, Wible CG (1991) Learning-related patterns of CA1 spike trains parallel stimulation parameters optimal

for inducing hippocampal long-term potentiation. Hippocampus 1: 181–192.

Pavlides C, Greenstein YJ, Grudman M, Winson J (1988) Long-term potentiation in the dentate gyrus is induced preferentially on the positive phase of theta-rhythm. Brain Res 439:383–387.

Ranck JB Jr (1973) Studies on single neurons in dorsal hippocampal formation and septum in unrestrained rats. Exp Neurol 41:461–555.

Robinson GB (1986) Enhanced long-term potentiation induced in rat dentate gyrus by coactivation of septal and entorhinal inputs: Temporal constraints. Brain Res 379:56–62.

Sainsbury RS, Harris JL, Rowland GL (1987) Sensitization and hippocampal type 2 theta in the rat. Physiol Behav 41:489–493.

Semba K, Komisaruk BR (1978) Phase of the theta wave in relation to different limb movements in awake rats. EEG Clin Neurophysiol 44:61–71.

Skaggs WE, McNaughton BL (1996) Replay of neuronal firing sequences in rat hippocampus during sleep following spatial experience. Science 271:1870–1873.

Skaggs WE, McNaughton BL, Gothard KM, Markus EJ (1993a) An information-theoretic approach to deciphering the hippocampal code. In: Advances in neural information processing systems (Hanson SJ, Cowan JD, Giles CL, eds), vol 5, pp 1030–1037. San Mateo, CA: Morgan Kaufmann.

Skaggs WE, Wilson MA, McNaughton BL (1993b) Spatial specificity of hippocampal place cells changes with phase of the theta cycle. Soc Neurosci Abs 19:795 (324.16).

Squire LR (1992) Memory and the hippocampus: A synthesis from findings with rats, monkeys, and humans. Psychol Rev 99:195–231.

Stewart M, Fox SE (1990) Do septal neurons pace the hippocampal theta rhythm? Trends Neurosci 13:163–168.

Suzuki SS, Smith GK (1987) Spontaneous EEG spikes in the normal hippocampus. III. Relations to evoked potentials. EEG Clin Neurophysiol 69:541–549.

Treves A, Rolls ET (1991) What determines the capacity of autoassociative memories in the brain? Network 2:371–398.

Tsodyks MV, Skaggs WE, Sejnowski TJ, McNaughton BL (1996) Population dynamics and theta rhythm phase precession of hippocampal place cell firing: a spiking neuron model. Hippocampus, in press.

Tulving E (1972) Episodic and semantic memory. In: Organization of memory (Tulving E, Donaldson WD, eds), pp 382–403. New York: Academic Press.

Vanderwolf CH (1988) Cerebral activity and behavior: Control by central cholinergic and serotonergic systems. Int Rev Neurobiol 30:225–340.

Vanderwolf CH, Leung LS (1983) Hippocampal rhythmical slow activity: A brief history and the effects of entorhinal lesions and phencyclidine. In: The Neurobiology of the hippocampus (Seifert W, ed), pp 275–302. London: Academic Press.

Vanderwolf CH, Kramis R, Gillespie LA, Bland BH (1975) Hippocampal rhythmical slow activity and neocortical low voltage fast activity: Relations to behavior. In: The hippocampus (Isaacson RL, Pribram KH, eds), vol 2: Neurophysiology and behavior, pp 101–128. New York: Plenum Press.

Wilson MA, McNaughton BL (1993) Dynamics of the hippocampal ensemble code for space. Science 261:1055–1058.

Winson J (1972) Interspecies differences in the occurrence of theta. Behav Biol 7:479–487.

Ylinen A, Bragin A, Nádasdy Z, Jandó G, Szabó I, Sik A, Buzsáki G (1995) Sharp wave-associated high-frequency oscillation (200 Hz) in the intact hippocampus: Network and intracellular mechanisms. J Neurosci 15:30–46.